BACHELOR

A combined optical and electrical approach for studying triplet-polaron quenching in organic phosporescent devices

Hu, Lan

Award date:
2017

A combined optical and electrical approach for studying triplet-polaron quenching in organic phosphorescent devices

Lan Hu[1]

[1]Department of Applied Physics, TU/e

September 12, 2017

Supervised by,
prof. dr. Reinder Coehoorn,
ir. Aart Ligthart.

Abstract

It was not immediately evident that organic electronics would be a breakthrough technology, however organic light emitting diodes (OLEDs) have gained market share rapidly, thanks to their wide colour gamut and high efficiency. Unfortunately, the theoretical efficiency limit is not yet reached in practice. This work will combine two approaches used to characterize organic light emitting diodes such that the present-day model, which uses the conventional rate equation for triplet exciton decay, can be improved. The first approach assumes a Gaussian distribution of energy states as basis for charge transport, whereas the second approach uses optical thin film analysis as a basis. The electrical simulations used a numerically efficient one-dimensional continuum drift-diffusion model. For the optical approach Setfos was used. To analyse the photoluminescence caused by a laser source and measured with a photo detector. The goal is, to combine polaron density simulations and an optical analysis of real world devices in order to investigate the validity of the conventional rate equation. It is first shown in this work that the measured electrical characteristics of symmetric tris(4-carbazoyl-9-ylphenyl)amine (TCTA) devices are in good agreement with the electrical simulation results at voltages starting from 5 V up to 10 V. With help of the optical model, it is shown that the effective triplet-polaron rate coefficient is not constant as function of the current density. This implies that current analysis methods, which are based on the rate equation, might not give a meaningful prediction of the efficiency of OLEDs.

Contents

1 Introduction **1**
- 1.1 OLEDs a light source and their applications . . . 1
- 1.2 Organic semiconductors . . . 1
- 1.3 OLED device structure . . . 1
- 1.4 Motivation of this work . . . 3
- 1.5 Aim of this work . . . 3

2 Theoretical background **4**
- 2.1 Polaron and exciton . . . 4
- 2.2 Charge transport . . . 4
- 2.3 Quenching mechanism . . . 5
- 2.4 Triplet-polaron quenching and triplet-triplet annihilation . . . 6
- 2.5 Photon generation in phosphorescent organic devices . . . 6
- 2.6 Electrical calculation model . . . 6
- 2.7 Optical Analysis . . . 8

3 Experimental setup **10**
- 3.1 Equipment device fabrication . . . 10
- 3.2 Equipment device characterization . . . 10
- 3.3 Calibration . . . 10
- 3.4 Molecular orbitals of materials . . . 11
- 3.5 Device fabrication . . . 12
- 3.6 Device pattern and numbering . . . 12
- 3.7 Phasor analysis . . . 13
- 3.8 Electrical characterization . . . 14
  - 3.8.1 Ambient temperature measurement . . . 14
  - 3.8.2 Temperature dependent measurement . . . 14
  - 3.8.3 Impedance characterization . . . 14
- 3.9 Optical simulation . . . 14

4 Results and discussion **16**
- 4.1 Device thickness . . . 16
- 4.2 Ambient J-V measurements . . . 18
- 4.3 Temperature dependent steady state measurements . . . 21
- 4.4 Carrier density . . . 22
- 4.5 Optical simulation . . . 23
- 4.6 Triplet-polaron quenching rate . . . 26

5 Conclusion **28**

Appendices **31**

A Cleaning procedures **31**
- A.1 Cleaning blank glass samples . . . 31
- A.2 Cleaning ITO glass samples . . . 31

B Error analysis **31**

C Emission spectrum of $Ir(ppy)_2acac$ **32**

D Mathematica script **33**

1 Introduction

In this chapter, the field of organic semiconductors and OLEDs will be introduced. Firstly, the important terminology used in OLED device physics will be explained. Secondly, the motivation of this work will be given. Lastly, the aim of this work will be defined.

1.1 OLEDs a light source and their applications

Artificial light sources like fire[1], incandescent lights, light-emitting diodes (LEDs) and now Organic light-emitting diodes (OLEDs) have been important light sources for humanity.

Nowadays OLEDS are widely used in televisions, smartphones, tablets and smartwatches. They are used in favor of their counterparts e.g. LCD, because of their wider color gamut and superior contrast ratio. Besides their better color reproduction characteristics, OLEDs also have superior energy efficiency. Lastly, OLEDs generally require less space (no need for backlight) and can be produced on flexible substrates, which allows curved screens. In general there are two types of OLEDs. The first type is based on polymers. The second type is based on small molecules, which most of the commercially available OLEDs, as well as the OLEDs studied in this paper are.

OLEDs are LEDs with an organic material as semiconductor, instead of typical semiconductors e.g. Gallium arsenide (GaAs). In order to create a suitable organic semiconductor, a high conductivity needs to be reached. This was achieved already in 1977 by π-conjugated polymers. For this discovery, the Nobel price was awarded in 2000 to Heeger, MacDiarmid, and Shirakawa.[2;3]

1.2 Organic semiconductors

Most of the organic semiconductors used nowadays are more or less disordered and are held together by van der Waals forces. This prevents charges to move like in semiconductor crystals like GaAs, but jump (hop) from one part of the polymer chain to the other. In normal semiconductors the electrons and holes, the counterpart of electrons, are delocalized (free) over the conduction and valence band. An electron in the valence band can be excited, by e.g. photon absorption, to the conduction band and it will leave a hole in the valence band. In organic semiconductors something similar happens. However the energy gap is due to a **lowest unoccupied molecular orbital** and **highest occupied molecular orbital**, in shorthand LUMO, HOMO respectively. The LUMO and HOMO are similar to conduction and valence band respectively.

1.3 OLED device structure

In order to achieve a completer picture of how OLED looks like, it is helpful to look at one of the early (and more simple) design of OLEDs depicted in Figure 1.1. Going from outside inwards, the outermost layer is the electrode. Usually the anode is optically transparent and cathode reflective. Most of the time ITO is used as the anode material. It has a high transparency in thin layers of tens up to a few hundreds of nm and has good hole injecting capability.[5] The following layers are the hole and electron injection layers (EIL and HIL). These layers improve device efficiency by decreasing or eliminating loss processes e.g. for hole injection. In this situation the HOMO of the EML is matched with the Fermi level of the anode, that is to bridge the gap of the energy levels between these two layers. The last layer is an emissive layer (EML), the organic layer. In the organic layer charges can recombine or interact with other charges or -typically- triplet excitons. In the case it interacts with a charge or a triplet exciton the energy is generally considered lost. This is called triplet-triplet annihilation (TTA) and triplet-polaron quenching (TPQ), respectively. In the case of charge recombination, the excess

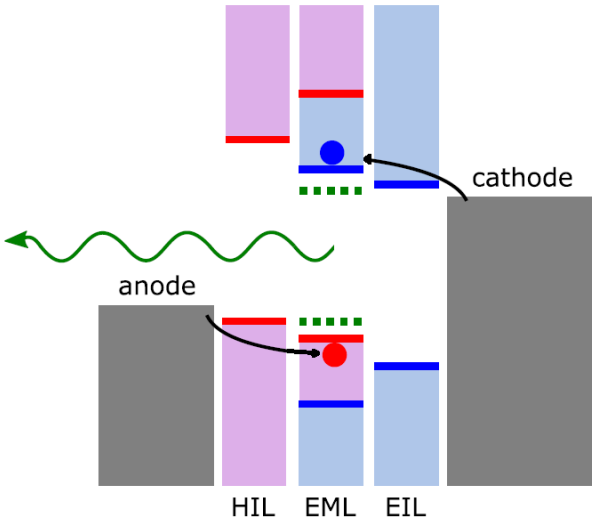

Figure 1.1: A schematic energy level diagram of a multilayer monochrome OLED stack. From left to right: the anode, the hole injection layer (HIL), the emissive layer (EML), electron injection layer (EIL) and cathode. The black arrows indicate the path of electrons and holes, it should be noted that the emissive layer consists out of both a hole and electron transporting layer, doped with dye molecules, of which the energy lives are indicated by the green dotted lines. Adapted from Ref. [4]

energy will be used for optical light radiation. Sometimes another layer between the HIL and EML is deposited for better device efficiency. These are called blocking layers.

1.4 Motivation of this work

In literature it is questioned whether the conventional rate equation describes exciton physics adequately. In this rate equation the loss processes are modelled to be linear with their respective densities. For triplet-polaron quenching studied in this work, it would be linear with the triplet and polaron density. This proportionality factor (rate coefficient) would include all other physical processes. However, there are strong indications that this view is oversimplified. For example, Coehoorn *et al.*[6] has shown there is a strong polaron density and field dependence in the exciton-polaron quenching rate coefficient.

Furthermore, in 2014 Van Eersel *et al.*[7] has shown by kinetic Monte Carlo (MC) simulations that, contrary to what often is assumed, not TTA, but TPQ is the leading loss process causing the roll-off for phosphorescent OLEDs. This implies an incorrect rate coefficient has been found in the works which consider TTA to be the leading loss process.

All of the above lead to this work, where the exciton physics as it is known to date is reassessed.

1.5 Aim of this work

In this work it is aimed to develop a optical OLED model and combine this with results of electrical simulations based on mechanistic models. That is, a model described by physical processes without any use of fitting parameters. Moreover, the optical model can be applied to improve stack design and the experimental method. The combined model will be used to characterize the underlying exciton physics of materials in OLEDs. The approach is a careful analysis of real-world measurement scenarios.

2 Theoretical background

In this chapter the theoretical background needed to have a basic understanding of the physics in organic light emitting diodes is given. Firstly, two key terminologies are explained. Secondly, a short introduction into charge transport is given. Thirdly, two types of charge transfer will be explained and its consequences in loss processes. Fourthly, a short overview of the formulas used in the calculation method is given. Lastly photon generation in OLEDs will be described and analysed in an au courant manner.

2.1 Polaron and exciton

Before discussing the loss processes observed in organic light emitting diodes (OLEDs), a short introduction to the charge carrier transport in organic semiconductors will follow, beginning with two important terminologies.

In condensed matter a **polaron** is a quasi-particle used to describe the combination of a moving lattice distortion and a charge. However, in the field of organic semiconductors a missing or an additional electron on a chromophore is often referred to as negative polaron or positive polaron.[8] Where the term chromophore refers to the part of a molecule where optical transitions are possible. The distortion (in case of organic semiconductors) is of intra-molecular nature.

The term **exciton** was coined to describe electron-hole pairs which are strongly bound to the molecules. For typical organic molecular materials, the permittivity is low so that Coulomb and exchange interaction have a significant influence. As a result, excitation leads to so-called Frenkel excitons, or in other words, strongly bound electron-hole pairs.[9] In this work only one process that leads to excitons are considered: optical excitation. Optical excitation might occur when light is absorbed by the molecule, while electrical creation of a exciton might occur when a carrier hops to a preoccupied molecule with a carrier of opposite charge. This however will not occur in the single carrier (hole-only) devices studied in this work. Following up will be an explanation of the charge transport inside disordered organic materials.

2.2 Charge transport

The structure of organic semiconductors used nowadays is generally disordered due to irregular deposition of molecules and structural distortion in polymer chains.[10] The disorder causes charges to be localized on single molecules or parts of the molecule, these are then identified as sites whose energy is Gaussian distributed. For organic semiconductors the standard deviation (σ) is typically 80 - 150 meV[11]. Charges are able to move from site i to j by hopping. The hopping rate ($r_{i,j}$) in the Miller-Abrahams formalism is given as,[12]

$$r_{i,j} = \nu_0 \exp\left(-2\gamma|R_{ij}|\right) \begin{cases} \exp\left(-\frac{E_j - E_i}{k_\mathrm{B}T}\right), & \text{if } E_j > E_i \\ 1, & \text{else.} \end{cases} \tag{2.1}$$

Here ν_0 is a hopping attempt rate, γ the inverse localization radius, R_{ij} the distance between sites, E_i and E_j are the energy of the respective sites, k_B the Boltzmann constant and T the temperature.

The charges in the symmetric device depicted in Figure 2.1 will be injected from the anode into the HOMO. Due to the high energy gap between the LUMO and the cathode, no electron charge carriers will be injected. Therefore, these symmetric devices are also called hole-only devices. These holes or rather hole-polarons are then transported through the active layer by either diffusion or drift, which results in a current to flow. Diffusion transport is a result of gradients in the charge carrier density or carrier density in short ($n_p(x)$) and drift transport is as a result of applied electric field ($F(x)$).

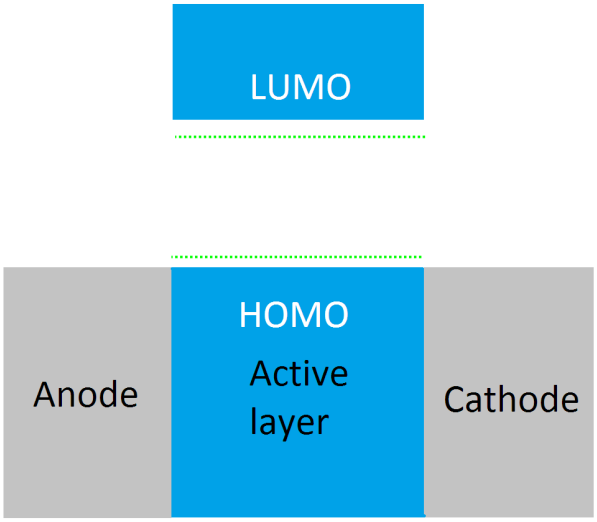

Figure 2.1: Schematic energy level diagram of a ideal symmetric device, i.e. no energy barrier between active layer and electrodes. With the electrodes in gray and the active layer in blue. The energy level for the guest molecules are given in green.

In phosphorescent OLEDs, organometallic dye molecules are introduced into the host, the material of the active layer. These typically have a different HOMO than their host. When a current is passed through a device, e.g. an OLED, charge carriers will become trapped at the dye molecules and eventually recombine with their opposite charge carriers. However, in the device in Figure 2.1 and studied in this work, no electrons are injected and the charges stay for very long times on the guest molecules. The long trapping times lead to a reduced mobility in doped materials. Despite the reduced mobility, organometallic dye molecules are used in order to achieve a 100% internal quantum efficiency.[13]

2.3 Quenching mechanism

The excitons can be in two states called: singlet and triplet excitons. Singlet excitons have a spin quantum number of 0 and triplet excitons have a spin quantum number of 1. Quenching of an exciton mainly occurs for triplet state excitons due, but not limited, to short singlet state exciton-lifetime and rapid intersystem crossing in typical phosphorescent OLED devices. When excitons interact with polarons the excitons are quenched, this means the energy is not available any more for a radiative decay. The interaction between exciton and polaron is governed by two possible mechanisms. Both mechanisms follow a non-radiative energy transfer and are different in their quantum chemical coupling interaction. This energy transfer can be given oversimplified as,

$$\mathrm{D}^* + \mathrm{A} \xrightarrow{\text{coupling interaction}} \mathrm{D} + \mathrm{A}^*, \tag{2.2}$$

with D the donor molecule, A the acceptor molecule and * indicating an excited state.[8]

One of the possible mechanisms is Förster-mediated energy transfer. In Förster mediated transfer, the excitation energy will be transferred to an acceptor molecule via dipole-dipole coupling. This interaction is often considered a long range interaction.[14] In order to quantitatively describe this process, it is useful to know the rate. The Förster rate is defined as,

$$r_F = \tau_f^{-1} \left(\frac{R_F}{R} \right)^6, \tag{2.3}$$

with τ_f lifetime of the donor in the absence of an acceptor, R_F the Förster radius and R the distance between donor-acceptor.[15]

The second mechanism is a Dexter-mediated energy transfer. Here the energy transfer happens through an exchange-type of coupling. In order to achieve a non-zero exchange, wavefunction overlap is necessary.[15] For Dexter transfer the rate is given by,

$$r_D = h \cdot K^2 \cdot J \cdot \exp\left(\frac{-2R}{\lambda_{ex}}\right), \tag{2.4}$$

with h Planck's constant, K a constant in terms of energy, λ_{ex} the wavefuntion decay length for excitons and J the spectral overlap between donor and acceptor.

Comparing Equation (2.3) and (2.4), it can be noted that a Förster-mediated energy transfer is generally seen as a long-range energy transfer process and a Dexter-mediated energy transfer is generally seen as a short-range energy transfer process. Furthermore, it should be noted that due to the organometallic phosphorescent dye molecules. Consequently, the devices studied in this work, show a strong spin-orbit coupling. This results in mixing of singlet and triplet states, breaking spin-selection rules.[14]

2.4 Triplet-polaron quenching and triplet-triplet annihilation

The aforementioned mechanisms in Section 2.3, lead to a loss of excitons. This will be collectively called triplet-polaron quenching (TPQ) if this donor is an exciton with triplet character and the acceptor of the polaronic species. It is called triplet-triplet annihilation (TTA) if both donor and acceptor are excitons with triplet character.

2.5 Photon generation in phosphorescent organic devices

Consider a system of (only) triplet excitons, characterized by a time and position dependent concentration.[16] The time evolution of the triplet density is generally given by the rate equation[9;14;16],

$$\frac{\partial n_T(x,t)}{\partial t} = G(x,t) - \Gamma \cdot n_T(x,t) - k_{\mathrm{TTA}} \cdot n_T^2 - k_{\mathrm{TPQ}} \cdot n_T \cdot n_P, \tag{2.5}$$

with x the position, t the time, G a triplet generation term, $n_T(x,t)$ the triplet density, $\Gamma = \Gamma_r + \Gamma_{nr}$ the overall exciton decay rate in absence of any losses, also known as $\frac{1}{\Gamma} = \tau$ the phosphorescent recombination lifetime of a triplet state, with Γ_r, Γ_{nr} the radiative and non radiative decay rate respectively, the loss processes are then given by TPQ and TTA with k_{TTA} the TTA rate coefficient, k_{TPQ} the TPQ rate coefficient and n_p the polaron density.[17]

2.6 Electrical calculation model

The same calculation method for the Gaussian disorder model (GDM) as described in the paper of Van Mensfoort and Coehoorn[11] is used. Their method was used in order to simulate hole-charge transport in single-layer devices.

In the GDM model it is assumed, that transport in organic semiconductor devices follow a Gaussian distribution of energy states. In this model the energy level at neighboring sites are assumed to be uncorrelated. The corresponding Gaussian density of states (DOS) can be formulated as,

$$N(E) = \frac{N_t}{\sqrt{2\pi\sigma^2}} \exp\left(\frac{-E^2}{2\sigma^2}\right), \tag{2.6}$$

with N_t the site density, σ the width of the Gaussian DOS (standard deviation) and E the energy of a certain level.

In the extended Gaussian disorder model the carrier density as function of the position ($n(x)$), enhances the diffusion and mobility. Since there is a carrier concentration dependence, careful analysis is needed in order to solve the drift-diffusion equation, given as,

$$J = e\mu(x)n(x)F(x) - eD(x)\frac{\mathrm{d}n(x)}{\mathrm{d}x}, \tag{2.7}$$

with J the current density, $\mu(x)$ the enhanced mobility as function of x, $F(x)$ the electric field and $D(x)$ the diffusion coefficient as function of x, which follows from the generalized Einstein equation for a Gaussian DOS, see Appendix A in the work of Van Mensfoort and Coehoorn [11].

The carrier density and field are related via the Poisson equation,

$$\epsilon\frac{\mathrm{d}F(x)}{\mathrm{d}x} = e \cdot n(x), \tag{2.8}$$

with ϵ the permittivity and e the electron charge.

Similar to Pasveer *et al.* [18], Van Mensfoort and Coehoorn [11] factorized the enhanced mobility function such that,

$$\mu(T, n, F) = \mu_0^* \exp\left(-C\hat{\sigma}^2\right) \cdot g_1(c, T) \cdot g_2(F, T), \tag{2.9}$$

with $g_1(c, T)$ the dimensionless carrier density dependent mobility enhancement factor, $c = \frac{n}{N_t}$ the carrier concentration, μ_0^* the mobility in the limit of zero electric field and zero carrier density and infinite temperature, C a parameter and $\hat{\sigma}$ the dimensionless disorder parameter given by,

$$\hat{\sigma} = \frac{\sigma}{k_\mathrm{B}T}. \tag{2.10}$$

The dimensionless carrier density dependent mobility enhancement factor is given by,

$$g_1(c, T) = \exp\left[\frac{1}{2}(\hat{\sigma}^2 - \hat{\sigma})\,(2c)^\delta\right] \quad \text{for} \quad c \leq 0.1, \tag{2.11a}$$

$$g_1(c, T) = g_1(T, 0.1) \quad \text{for} \quad c > 0.1, \tag{2.11b}$$

and the dimensionless field dependent mobility enhancement factor is given by,

$$g_2(F, T) = \exp\left[A(\hat{\sigma}^{3/2} - 2.2)\left(\sqrt{1 + B\left(\frac{Fea}{\sigma}\right)^2} - 1\right)\right] \quad \text{for} \quad F \leq \frac{2\sigma}{ea}, \tag{2.12a}$$

$$g_2(F, T) = g_2\left(\frac{2\sigma}{ea}, T\right) \quad \text{for} \quad F > \frac{2\sigma}{ea}, \tag{2.12b}$$

with $a = N_t^{-1/3}$ the average inter-site distance, c the carrier concentration and δ is given by,

$$\delta = 2 \cdot \frac{\ln\left(\hat{\sigma}^2 - \hat{\sigma}\right) - \ln\left(\ln\left(4\right)\right)}{\hat{\sigma}^2} \tag{2.13}$$

The A, B and C parameters can be retrieved from *ab initio* calculations, these can include the morphology, the molecular on-site energies, reorganization energies and charge transfer integrals. [19]

2.7 Optical Analysis

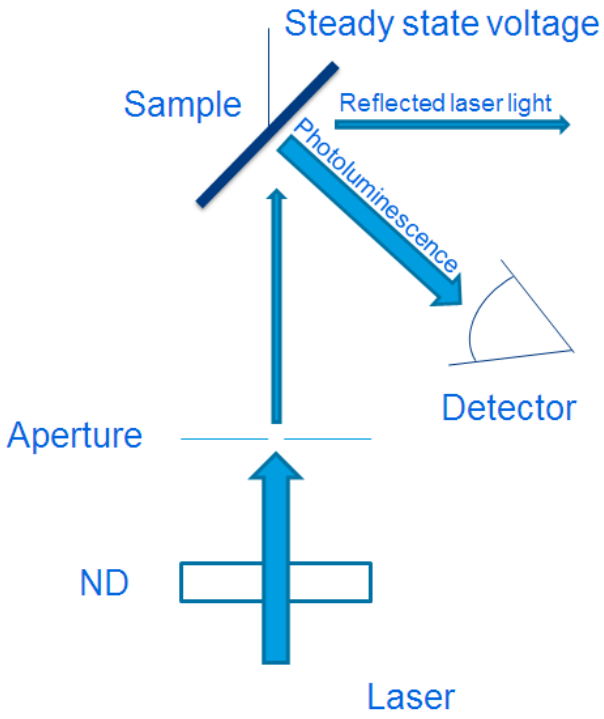

Figure 2.2: Schematic overview of a typical photoluminescence experiment. A pulsed laser is shot at the sample. The laser light travels through ambient air into a neutral density filter (ND). Afterwards, the beam width is limited by an aperture in order to fit within the active device area. The reflected laser light is reflected off the sample and the emitted phosphorescent light is captured by an detector. Furthermore, the sample bias voltage is varied.

In an TPQ experiment a short laser pulse travels through a neutral density filter (ND) which allows the laser intensity to be varied using different ND filters. Then the laser pulse travels through a aperture such that the laser spot stays within the active region of the device. The reflected laser light escapes, while the phosphorescent light is captured by a detector. This process -light emission after photon absorption- is called photoluminescence (PL). Therefore, this setup will be called a PL setup and is depicted in Figure 2.2.

For a photodiode detector at reverse bias, the measured photo current (signal) is linear with the irradiance and also linear with the intensity when the detector is stationary. It is expected that the photoluminescence (PL) will decrease with increasing current density.[20] It is also expected that the leading loss process in phosphorescent devices is TPQ.[7] This implies that TPQ is significantly larger than TTA, because TTA is negligible at the low exciton concentration of the studied devices. Accordingly, the time evolution of the triplet density in the studied devices can be approximated as,

$$\frac{\partial n_T(x,t)}{\partial t} = G(x,t) - \Gamma \cdot n_T(x,t) - k_{\mathrm{TPQ}} \cdot n_T \cdot n_P, \tag{2.14}$$

Furthermore, it is measured that the PL intensity at a certain J decreases exponentially over time, hence the solution of Equation (2.14) is,

$$n_T(x,J,t) = n_0(x) \exp\left(\frac{-t}{\tau'}\right), \tag{2.15a}$$

$$\frac{1}{\tau'} \equiv \frac{1}{\tau} + k_{TPQ} \cdot n_p(x, J), \tag{2.15b}$$

with $n_0(x)$ the triplet density profile at $t = 0$ as function of the position, which is called incoupling from now on. The triplet density profile at $t = 0$ profile is generated as consequence of a short laser pulse. That means the illumination time is much smaller than the triplet lifetime ($\tau = 1.37\,\mu s$), but also assumes the absorption time to be much smaller than the triplet lifetime.

It should be noted that the triplet lifetime in real devices is modified by the well known Purcell effect [21], which has not been taken into account here.

The emission intensity (I_{PL}) is proportional to n_T.[14] If the dye molecules are homogeneous doped into the active layer with thickness L, the resulting emission is from the whole active layer. Therefore, the relation between intensity measurements combined with Equation (2.14) can be given as,

$$I_{PL}(t, J) \propto \int_0^L \eta_{out}(x) n_0(x) \frac{\exp(\frac{-t}{\tau'})}{\tau}\, \mathrm{d}x, \tag{2.16}$$

with $\eta_{out}(x)$ the outcoupling efficiency as function of the position, i.e. the efficiency of conversion of internally generated radiation into far-field measurable optical power.

The PL efficiency is found by the time integral of the intensity from 0 to ∞ and can be normalized by a reference measurement at $J = 0$, which results in,

$$\frac{\eta_{PL}(J)}{\eta_{PL}(J=0)} = \frac{\int_0^L \eta_{out}(x) n_0(x) \frac{\tau'}{\tau}\, \mathrm{d}x}{\int_0^L \eta_{out}(x) n_0(x)\, \mathrm{d}x}. \tag{2.17}$$

The left-hand side is a quantity that can be measured by a PL experiment by integrating the transient measurement. The outcoupling and incoupling will follow from optical simulations in Section 4.5. Furthermore, the effective lifetime of a triplet state is modified due to TPQ. However, in case of the reference measurement ($J = 0$), TPQ is expected to be 0. All unknowns are determined by either measurement or optical simulations and only leaves k_{TPQ} to be determined. It should be noted that the τ' is a function of the position, hence Equation 2.17 can not be simplified any further. As a consequence, the TPQ rate coefficient needs be solved with a numerical solver, e.g. *Mathematica*.

3 Experimental setup

The aim of this work is to extend the calculational model with an optical model. First, the materials and machine used will be enumerated, the calibration method will be explained. Furthermore, the processed OLED device will be described. Next, the electrical characterization method. Lastly, an analysis of a PL setup and the needed optical simulation will be given.

3.1 Equipment device fabrication

An Ångström vacuum deposition system, with serial number: 01818-2 was used to deposit the following materials: tris(4-carbazoyl-9-ylphenyl)amine (TCTA) produced by Luminescence Technology, product number: LT-E 207; molybdenum trioxide (MoOx); aluminium; $Ir(ppy)_2acac$. The spinner was made by Headway Research, has the serial number: PW3202199-D and was used to spincoat Poly(3,4-ethylenedioxythiophene) polystyrene sulfonate (PEDOT:PSS) produced by Heraeus, product number: Clevios P VP.AI 4083. Next, a Bruker DektakXT, with serial number: 10089828 was used to determine the thickness of a layer.

3.2 Equipment device characterization

Firstly, for the steady state current-voltage measurements a Keithley sourcemeter 2400, with serial number ELI 5901-1130 was used. Secondly, for the impedance measurements a Solartron SI 1260 impedance/gain-phase analyzer was used. Lastly an Omega Engineering monogram, with serial number: ELI 6101-0067 was used to determine the temperature of the thermocouple.

3.3 Calibration

To set up the organic deposition by evaporation machine the correct tooling number is needed for accurate deposition. The aforementioned machine will be called evaporator from now on. To find the tooling number, clean blank glass samples were used. The cleaning procedure can be found in Table 2 in Appendix A.1. On the samples a thin piece of kapton tape was applied. Afterwards a layer with an certain material was evaporated on the samples, by removing the kapton tape and analysing these samples with the Dektak, the measured thickness can be determined. With the measured thickness the new tooling number can be determined according to,

$$[\text{tooling number}]_{\text{new}} = \frac{[\text{measured thickness}]}{[\text{theoretical thickness}]} \cdot [\text{tooling number}]_{\text{old}}. \tag{3.1}$$

TCTA
The following settings were used for the tooling of TCTA, a deposition layer of 100 nm, with an old tooling number of 36.5. The average thickness of the glass samples with TCTA is 71.5 ± 1.2nm. With help of Equation (3.1), a tooling number of 26.1 ± 0.4 is found.

MoOx
The following settings were used for the tooling of MoOx, a deposition layer of 50 nm, with an old tooling number of 61. An average thickness of 38 ± 2 nm is found. Again with help of Equation (3.1), a tooling number of 53 ± 3 is found.

Aluminum
The following settings were used for the tooling of aluminum, a deposition layer of 50 nm, with an old tooling number of 32. An average thickness of 29 ± 1 nm is found. Again with help of Equation (3.1), a tooling number of 38 ± 1 is found.

3.4 Molecular orbitals of materials

In order to gain insight whether the layers have good or bad injection into the following layers, the energy levels of molecular orbitals will be given below. The injection into the following layers will be considered good if the difference between energy levels of the materials is up to a few tenths of eV's.

The energy levels of the molecular orbitals of the materials TCTA and $Ir(ppy)_2acac$ can be found in Table 1. It should be noted that from previous ultraviolet photoelectron spectroscopy (UPS) an HOMO of 5.1 eV has been found for $Ir(ppy)_2acac$, contrary to the value of 5.6 eV found in literature.[22]

In Figure 3.1 the structural formula of PEDOT:PSS as well as TCTA can be found. These organic materials indeed show π-conjugated molecules.

The HOMOs of the matrix stack depicted in Figure 3.3 is given in Figure 3.2. It should be noted that the energy gap between TCTA and MoOx is relatively small and a good injection of holes is expected.

Table 1: Energy levels of the highest occupied molecular orbital (HOMO) and lowest occupied molecular orbital (LUMO) of TCTA and $Ir(ppy)_2acac$. Data retrieved from Ref.[22;23].

Material	TCTA	$Ir(ppy)_2acac$
HOMO (eV)	5.6	5.1/5.6
LUMO (eV)	2.4	3

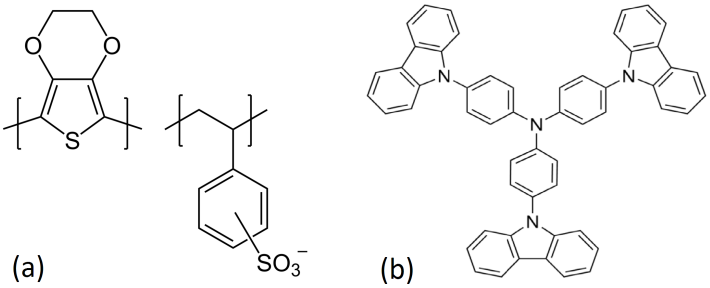

Figure 3.1: Structural molecule formulas for (a) Poly(3,4-ethylenedioxythiophene) polystyrene sulfonate (PEDOT:PSS) and (b) tris(4-carbazoyl-9-ylphenyl)amine (TCTA).

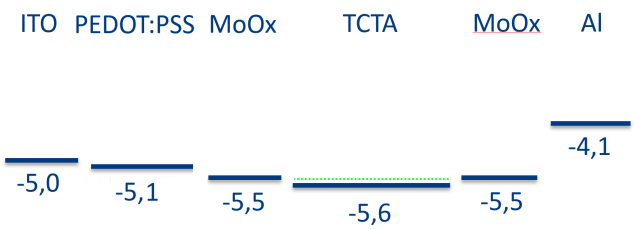

Figure 3.2: Schematic energy level diagram of the stack given in Figure 3.3. The Fermi energies of ITO, PEDOT:PSS, MoOx and aluminium (Al) are given by a dark blue bar. The HOMO of TCTA is also given by a dark blue bar and the HOMO of the dopant $Ir(ppy)_2acac$ is given by light green dots. The ITO layer is used as the anode and Al as the cathode. Adapted from Ref.[24]

3.5 Device fabrication

The clean ITO samples were transferred into an inert atmosphere (nitrogen). Inside the glove-box, PEDOT:PSS of 50 nm thickness was spin coated, with the spinner set at 3000 RPM and a rotation time of 60 seconds. Afterwards they were annealed in the same atmosphere for 20 minutes at 135 ° C. After annealing the samples were transferred into the Ångström vacuum deposition system also in nitrogen atmosphere. With a square mask two layers of MoOx (10 nm) with one layer of TCTA in between was deposited. Afterwards an patterned mask was used to deposit a patterned layer of 100 nm aluminum. The devices either had 150 nm or 135 nm TCTA. While some of the 150 nm devices had a 4 wt. % doping of $Ir(ppy)_2acac$, these will be referred as devices with dye molecules and the undoped devices as devices without dye molecules. The deposition rate of the materials was, in the same order, 0 5Å/s, 2Å/s and 2Å/s. The described order of layers follows the order given graphically in Figure 3.3.

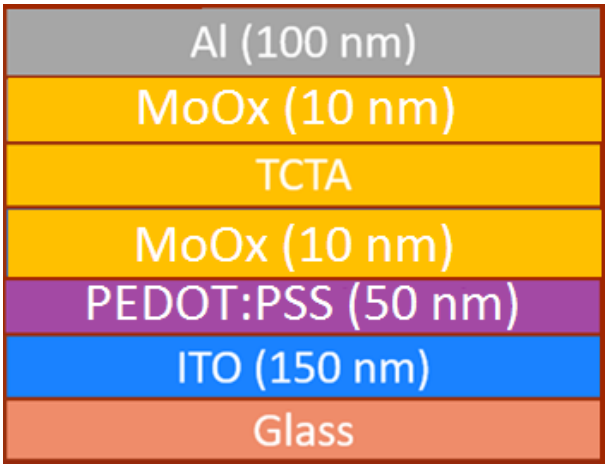

Figure 3.3: (a) Cross section of the matrix stack, (b) schematic energy level diagram of the matrix stack. In order of deposition which is from (a) bottom to top, (b) left to right, ITO, PEDOT:PSS, MoOx, TCTA, MoOx and aluminum, with thicknesses of 150 nm, 50 nm, 10 nm, various, 10 nm and 100 nm respectively.

3.6 Device pattern and numbering

Every substrate has four anode's and cathode's, resulting in four cross-sections, with two different area's, due to different electrode area. These will be numbered according to "area-index", with area the area of the device in mm and index the first or second device of a certain area. Starting from the upper-left corner the numbering clockwise, will be 9-1, 16-1, 9-2 and 16-2. A graphical representation can be found in Figure 3.4.

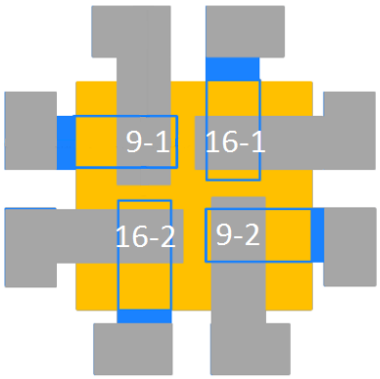

Figure 3.4: In blue ITO, in yellow MoOx and in gray aluminum. The order of layers is from bottom to top, blue, yellow, gray. The blue lines on the MoOX layer shows the ITO underneath TCTA. Whereas the colors are chosen according to their mask as described in Section 3.6. The order of device numbering started at the left corner and is clockwise: 9-1, 16-1, 9-2 and 16-2. Adapted from Ref.[25]

3.7 Phasor analysis

In order to measure the capacitance and resistance of devices, one can use phasor calculus as a tool. After exciting devices with a sinusoidal signal and measuring the current and voltage characteristics the impedance can be found.

To represent the complex ratio of voltage to current, the impedance ($\vec{Z}$) is used and is given as,

$$\vec{Z} = \frac{\vec{V}}{\vec{I}}, \tag{3.2}$$

with $\vec{V}$ the voltage in volt, $\vec{I}$ the current in ampere. In Cartesian form, the impedance can be written as a vector in the complex plane as,

$$\vec{Z} = R + iX, \tag{3.3}$$

with R the resistance, $i = \sqrt{-1}$ and X the reactance. An equally valid formulation of Equation (3.3) as a complex valued function is,

$$\vec{Z} = Z \cdot e^{i\theta}. \tag{3.4}$$

The formulation of Equation (3.4) follows from Euler's formula where any complex quantity can be expressed as a complex exponential, with θ the angle of $\vec{Z}$.

Ideal capacitive and inductive elements induce a phase shift with respect to a sinusoidal varying voltage these elements decrease or increase the reactance. A capacitor causes the current to phase shift $+90°$ relative to the voltage, while an inductor causes to phase shift $-90°$ relative to the voltage. The reactance of a capacitor can be defined as,

$$X_C = -\frac{1}{\omega C}, \tag{3.5}$$

with ω the angular frequency and C the capacitance. For completeness the reactance of an inductor is given,

$$X_L = \omega L, \tag{3.6}$$

with ω as defined before and L is the inductance.

3.8 Electrical characterization

In order to verify to calculation model, current density-voltage (J-V) measurements are done at various temperatures. The measurements will be then compared to simulation results of the calculation model, the parameters of the calculation model concerning the enhancement functions for TCTA were retrieved from the work of Massé *et al.*[19], these are as follows, $B = 1.9$, $C = 0.4$, $A \cdot B = 0.81$, $\sigma = 0.136\,\mathrm{eV}$ and $\mu_0^* = 7.6 \times 10^{-6}\,\mathrm{m^2/Vs}$. The other parameters, which are device quantities are chosen to be, $T = 300$ K and $\epsilon_r = 3$ for TCTA. Furthermore, the L of the devices with 135 nm TCTA and 150 nm TCTA doped with 4 wt. % $Ir(ppy)_2acac$ is confirmed by impedance measurement.

3.8.1 Ambient temperature measurement

For J-V measurements at ambient temperature a box made out of black plastic was used. This box was hermetically sealed. Furthermore, the electrodes at the inside were connected with BNC connectors on the outside. The box was hooked up via a coax cable with a sourcemeter and the data was saved with a custom Labview program.

3.8.2 Temperature dependent measurement

For J-V measurements at below ambient temperatures a steel box was used. The sample is cooled by a cooling plate with heat pipes connected to a heat sink. The heat sink is sealed from the sample and is cooled by a nitrogen flow. The nitrogen flow came from a dewar filled with liquid nitrogen and was manually regulated with a valve. Furthermore, the cooling plate was connected to a thermocouple with its output connected to a monogram. It is also connected to a sourcemeter and the data was saved with another custom Labview program.

3.8.3 Impedance characterization

The same box as in Section 4.2 was used, however now it was connected with a coax cable to the Solartron. At high frequencies the impedance of TCTA becomes negligible, thus the device starts behaving as an capacitor constructed of two parallel plates. From the phase and impedance measured by the Solartron the capacitance C' can be determined, whereas the capacitance (C') of 2 parallel plates is given by,

$$C' = \frac{\epsilon_0 \epsilon_r A}{L}, \tag{3.7}$$

with ϵ_0 the vacuum permittivity, ϵ_r the relative permittivity, A the area and L the thickness of the active layer. Equation (3.7) can be rewritten to,

$$L = \frac{\epsilon_0 \epsilon_r A}{C'}. \tag{3.8}$$

Which is an explicit equation for the thickness of the active layer.

Concerning the measurement settings, the devices will be measured at various bias voltages, ranging from -2 V to 2 V in steps of 1 V, the perturbation voltage is set at 10 mV. The frequency will as well be varied in order to verify whether the capacitance will converge to one value.

3.9 Optical simulation

In order to do thin film optical simulations, Setfos 3.2 of Fluxim was used. The matrix stack in Figure 3.3 was created in Setfos, with another layer of 10 nm between glass and ITO of SiO_2. In the software settings the option quenching was turned off and the complex refractive indices of aluminum and glass were retrieved from the Setfos program. Whereas the complex refractive

index of MoOx was retrieved from previous experiments. Furthermore, the refractive index of TCTA was calculated with Cauchy's equation, given as,

$$n(\lambda) = A^* + \frac{B^*}{\lambda^2} + \frac{C^*}{\lambda^4}, \tag{3.9}$$

with λ the wavelength in meters, n the real part of the complex refractive index, $A^* = 1.726$, $B^* = 0.005$ and $C^* = 0.003$ for TCTA. Also the complex part of the refractive index (k) was found by first calculating the attenuation coefficient (α) from absorbance measurements. Assuming linear attenuation in the active layer, α is given as,

$$\alpha = \frac{10^{A^\dagger}}{\ln(10)}, \tag{3.10}$$

with $A^\dagger$ the absorbance. Then k can be found by,

$$k = \frac{\lambda_0 \cdot \alpha}{4\pi} \tag{3.11}$$

Do note usually refractive indices of thin film materials are usually found by a more accurate technique called, spectroscopic ellipsometry.[26] They can as well be determined from transmittance and reflectance measurement, preferably in a integrating sphere.[27]

Kim *et al.*[28] reported that $Ir(ppy)_2acac$ had a preferential horizontal dipole moment. Since Setfos allows only a horizontal or a vertical dipole transition moment, it was assumed the emission was through (only) horizontal dipoles in Setfos. Furthermore, this simplification also simplified the interpretation of the complex refractive index of PEDOT:PSS. van Mensfoort *et al.*[29] reported different complex refractive indices for s or p polarized light. The refractive index was retrieved from Figure 5 of their work. Lastly, the experimental setup was fixed at an angle of 0 degrees with respect to the normal of the sample. As a consequence of this, vertical dipoles do not contribute to the emission anyway.

4 Results and discussion

The goal of this study is to confirm the calculation model and to be able to use the calculated position dependent polaron density as input of the optical model. This chapter focuses on the results of the experiment described in Section 3. Firstly, the thicknesses of the devices will be measured by impedance measurements. Secondly, results of transport measurement at various temperatures will be given. Thirdly, the results of the optical simulations will be explained. Lastly, the results of calculation model will be combined with the results of the optical model to characterize TPQ.

4.1 Device thickness

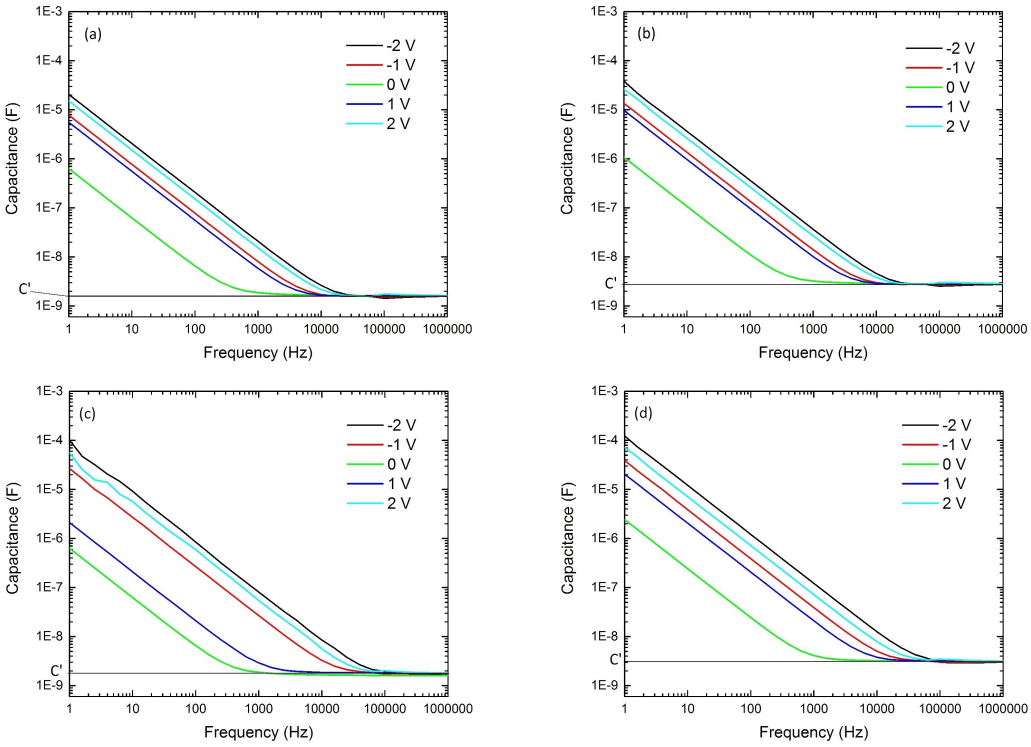

Figure 4.1: The capacitance as function of the frequency at various bias voltages. The perturbation voltage was chosen to have an amplitude of 10 mV. The devices used in (a) and (b) have 135 nm TCTA ideally and 9 mm and 16 mm active area, respectively. The devices used in (c) and (d) have 150 nm TCTA ideally and 9 mm and 16 mm active area, respectively. All devices, at various bias voltages converge to a certain capacitance given in grey.

Before verifying the calculational model with J-V measurements, the thickness needs to be confirmed by electrical characterization.

In Figure 4.1 it can be seen that the devices indeed converge to a certain capacitance at high frequencies for various bias voltages. The thicknesses of the active layers follows from Equation 3.8. For every device thickness one 9 and 16 mm area device were measured, furthermore ϵ_r is chosen to be 3. For the devices without dye molecules and ideally 135 nm thickness, a L of (134 $\pm$) 1 nm was found. For the devices with dye molecules and ideally a 150 nm thickness, a L of (150 $\pm$ 1) nm was found.

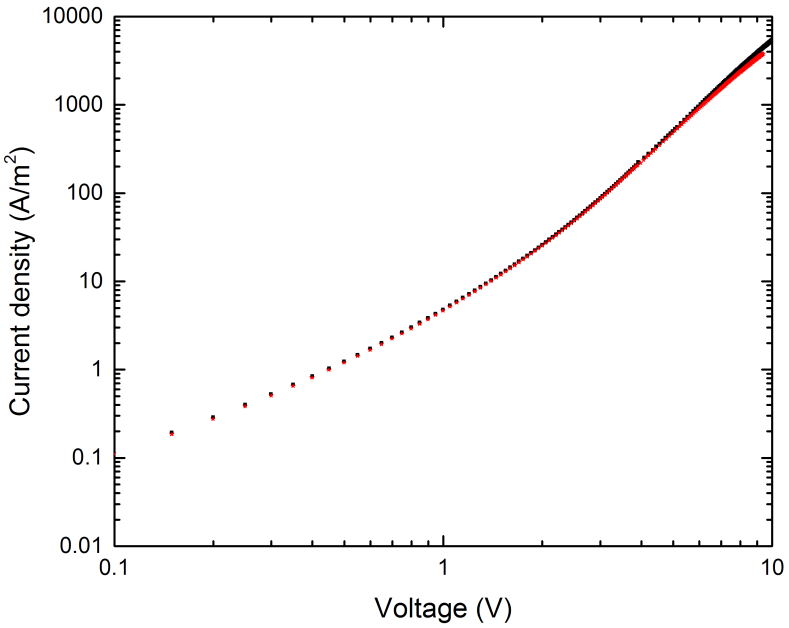

Figure 4.2: The current density as function of the voltage for various devices with 135 nm TCTA. In black devices with 9 mm active area and in red the devices with 16 mm active area.

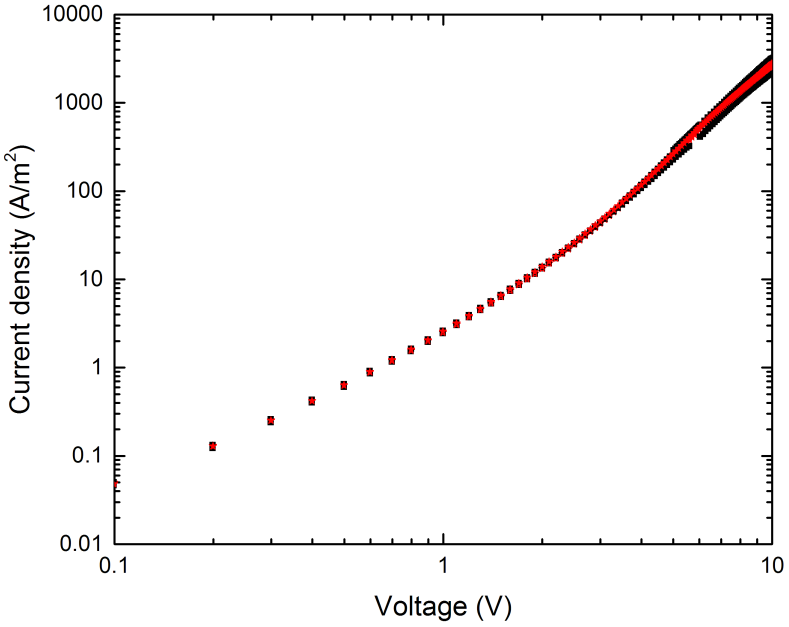

Figure 4.3: The current density as function of the voltage for various devices with 150 nm TCTA. In black devices with 9 mm active area and in red the devices with 16 mm active area.

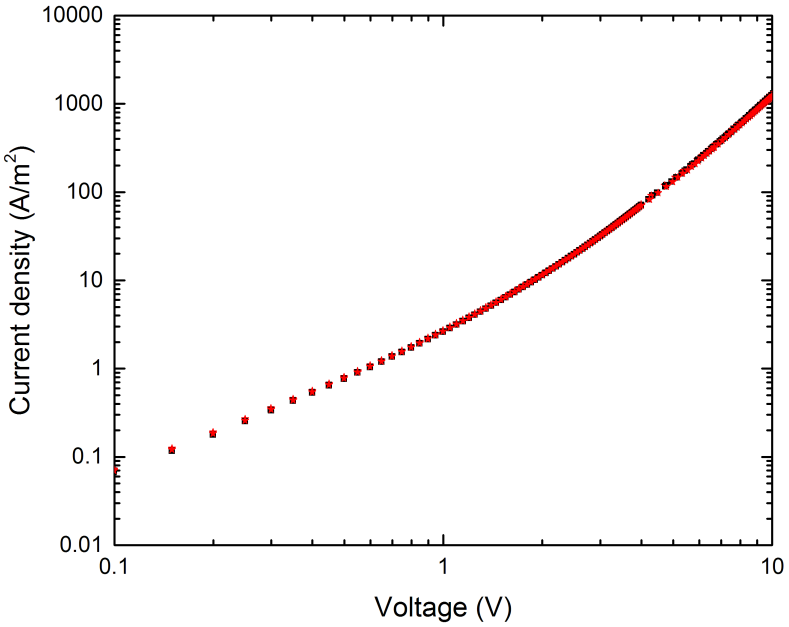

Figure 4.4: The current density as function of the voltage for various devices with 150 nm TCTA doped with 4 wt. % $Ir(ppy)_2acac$. In black devices with 9 mm active area and in red the devices with 16 mm active area.

4.2 Ambient J-V measurements

Previous experiments have shown a device yield of around 40-50%, while the J-V measurements between devices were inconsistent. It was suggested PEDOT:PSS could even out the surface roughness the ITO and MoOx interface, this lead to the new design studied in this work. In this new design, depicted in Figure 3.3, a PEDOT:PSS layer was brought between the ITO and MoOx. With this new device design the overlap of J-V characteristics between different devices on the same substrate should be improved.

Figures 4.2, 4.3 and 4.4 shows the J-V measurements of all four devices on three different substrates, these substrates have an active layer thickness of 135 nm without any dye molecules, 150 nm without dye molecules, 150 nm with dye molecules, respectively. All of the devices on a certain substrate are identical except for their dimensions. However, the current density is not a function of the area of the device. Hence, the devices with different area should show similar J-V characteristics.

In Figure 4.2 and Figure 4.3 the measurements between different devices show a lot of overlap. While the the measurement points are not exactly on top of each other, they have fairly similar J-V characteristics. The small disagreement between different devices can be due to, but not limited to, device heating, misaligned pattern mask or dust. Increase in the temperature can increase the current density. While a skewed pattern mask can decrease the area by 10%.

In Figure 4.4 all of the measurement points overlap each other very well, as expected of identical devices with different areas.

Next, In Figure 4.5 the experimental data is compared to the simulated J-V curve, found according to the method proposed in Section 2.6. The simulated J-V curve and the experimental data show good agreement at high voltages ($V > 5\,\mathrm{V}$), with progressively worse agreement at low voltages ($V < 5\,\mathrm{V}$). Since the parameters were chosen such that the resulting curves had good agreement with the 3D model (master equation) in the work of Massé *et al.*[19], the used

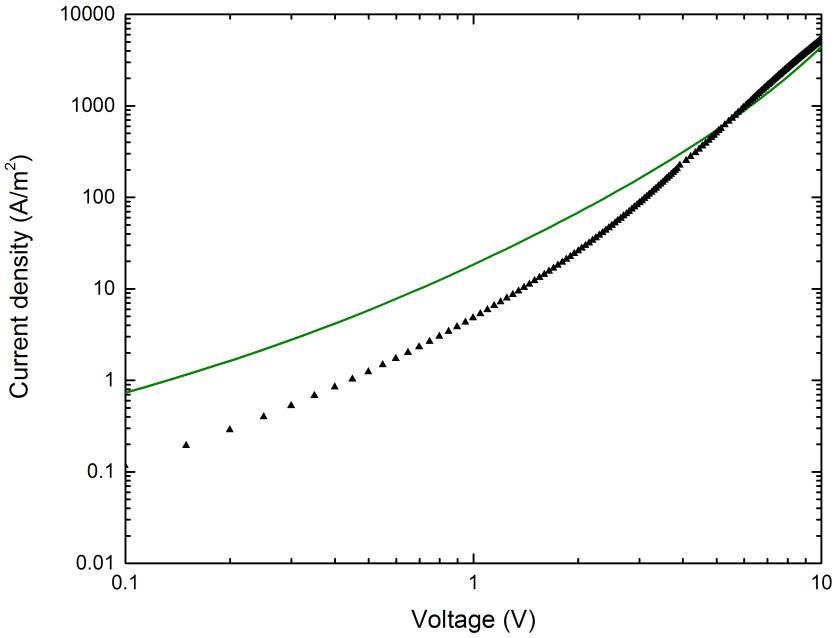

Figure 4.5: The current density as function of the voltage for a 135 nm TCTA device in black compared with simulation in green. The parameters used were as described in Section 3.8, the device parameters for the simulation was $L = 135$.

calculation method (1D model) does not take charge repulsion into account. This could imply that a higher mobility is expected than it will be found experimentally, resulting in a higher current density at low voltages, which is the case here.

Furthermore, in Figure 4.6 the devices with and without PEDOT:PSS are compared. The devices without PEDOT:PSS have a layer thickness of 160 nm, while the devices with PEDOT:PSS have a layer thickness of 150 nm. The devices with and without PEDOT:PSS have a similar change of slope of the J-V curve. It can be seen from Figure 4.6 that a higher current density is found for devices with PEDOT:PSS than without, this is in accordance with $J \propto L^{-3}$.[11] However, the difference between thicknesses is minimal and should not increase the current density for a thinner device by a factor 2. Consequently, this implies that using PEDOT:PSS indeed decreases possible ITO-MoOx interface defects by smoothing any irregularities which inhibit charge transport. This slight increase in current density for a thinner device can be seen as well in Figure 4.6 as the curved lines, with the same parameters as before with 150 and 160 nm layer thicknesses.

For the devices with PEDOT:PSS, with and without dye molecules are compared in Figure 4.7. For the simulations the same parameters are used as before, but with an active layer thickness of 150 nm. Once again for the devices without dye molecules good agreement is found with the simulations at high voltages. What this also implies, given that the calculation method described in Section 2.6 is correct, reliable polaron densities at high voltages can be extracted from this method. Meaning that k_{TPQ} can reliably be found with the analysis method described in Section 2.7 when the polaron density is used from the calculation method.

Lastly, in the devices with dye molecules, trap sites are introduced as a result of these dye molecules. Because of trap sites, the amount of polarons are quenched, however a good overlap of the HOMO TCTA and $\mathrm{Ir(ppy)_2acac}$ will result in a low degree of trapping. A low degree of trapping implies that the the permittivity basically stays the same and the current density does

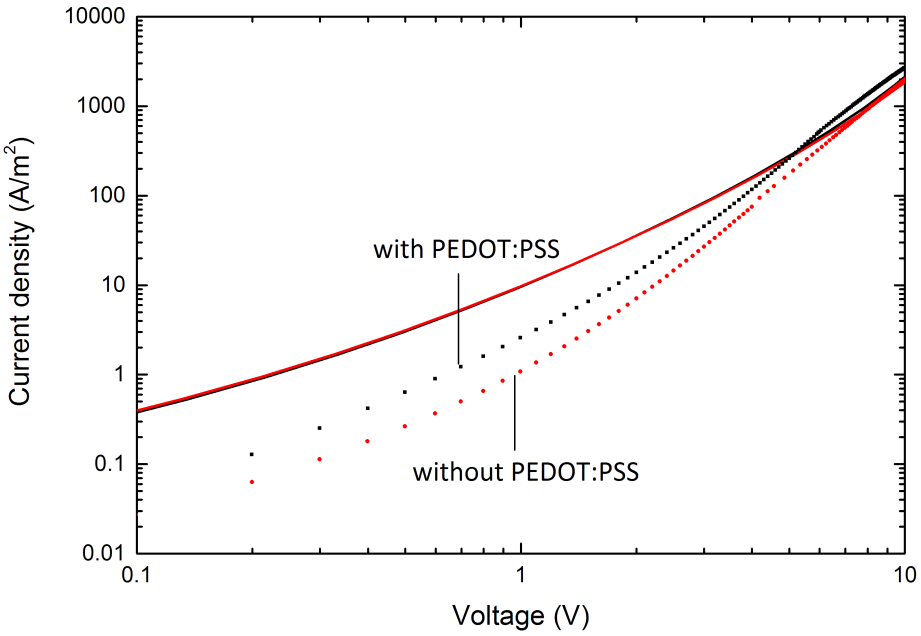

Figure 4.6: The current density as function of the voltage for a 150 and 160 nm TCTA device in black and red respectively, measurement are symbols and simulations are drawn with a solid line. The parameters used were as described in Section 3.8, the device parameters for the simulation was $L = 150$ and $L = 160$, respectively.

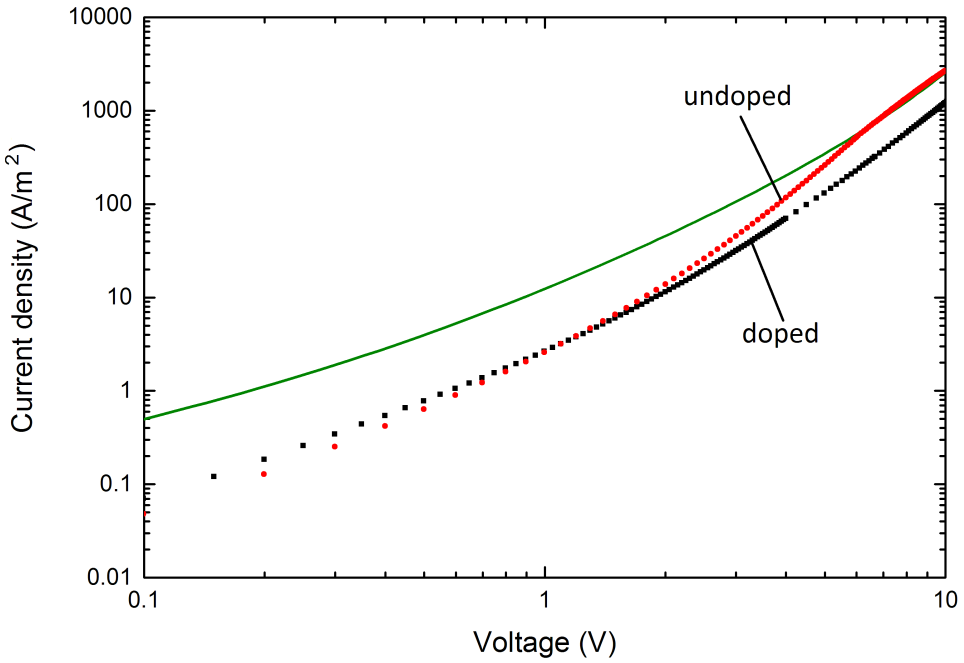

Figure 4.7: The current density as function of the voltage for a 150 nm TCTA device with (doped) and a device without (undoped) 4 wt. % ir(ppy)$_2$acac, measurement are black (doped) and red (undoped) symbols and the simulation is drawn with a green solid line. The parameters used were as described in Section 3.8, the device parameters for the simulation was $L = 150$.

not decrease a lot due to these trap sites. Previous UPS experiments have shown HOMO of 5.1 eV for $Ir(ppy)_2acac$, which leads to bad overlap of the HOMO of TCTA and $Ir(ppy)_2acac$. Hence a high degree of trapping was expected for $Ir(ppy)_2acac$ in TCTA. However, the current density of devices with dye molecule at 10 V in Figure 4.7 is only decreased by a factor 2 in comparison with the devices without dye molecules. Lastly, it should be noted that the degree of trapping should decrease at higher voltages, due to shifting of the energy level landscape. This effect is not observed and appears to be much more complicated in the case of organic semiconductors.

4.3 Temperature dependent steady state measurements

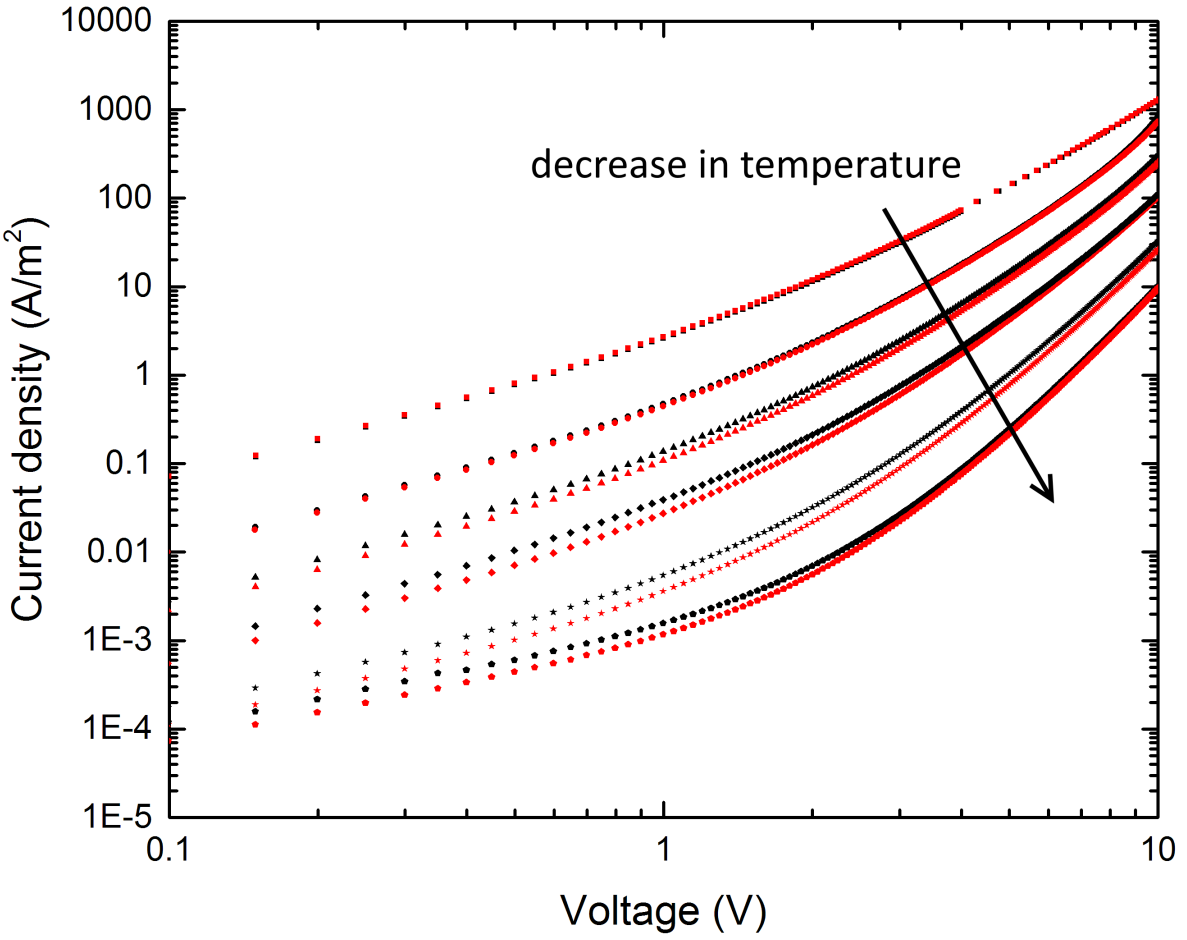

Figure 4.8: The current density as function of the voltage for a 150 nm TCTA device with 4 wt. % ir(ppy)$_2$acac at various temperatures. The 9 mm device is given in black and the 16 mm device is given in red, with the symbol square 300 K*, circle* 270 K*, triangle* 250 K*, diamond* 230 K*, star* 210 K *and pentagon* 190 K*. The parameters used were as described in Section 3.8, the device parameters for the simulation was* $L = 150$*.*

To verify the correct choice of σ, the width of the Gaussian DOS, temperature dependent measurements have been done. When scaling the temperature e.g. down, similar agreement with simulations and measurements need to be found as in Section 4.2. But, first the devices with different area are compared in Figure 4.8. After decreasing the temperature in steps, the J-V measurement points overlap each other less after every step, this is most notable in the low voltage region. It shows similar characteristics with a ferroelectric material, which

can show a spontaneous non-zero polarization when the applied electric fields are zero. After measuring at a certain temperature, the devices were not reverse biased before continuing to the next temperature. This implies, if indeed the material acts like a ferroelectric material, the measurement at low fields all show spontaneous polarization. This hysteresis effect becomes more noticeable at low temperatures, because the molecules are less disordered and the dipole moment of the molecules will become more ordered.

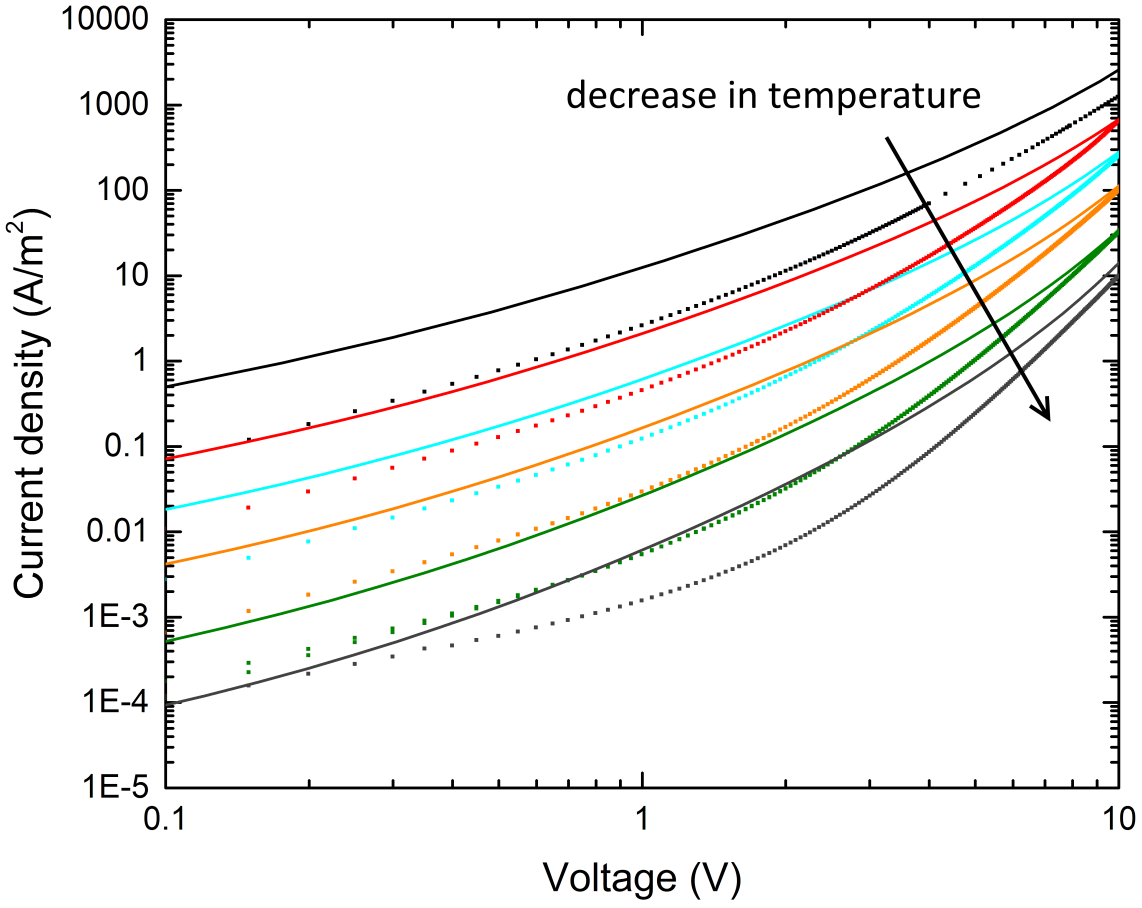

Figure 4.9: The current density as function of the voltage for a 150 nm TCTA device with 4 wt. % Ir(ppy)$_2$acac at various temperatures. The measurement is given in symbols, the simulation is given as a solid line and the temperature in various colours. This was colour coded according to, black 300 K*, red* 270 K*, turquoise* 250 K*, orange* 230 K*, green* 210 K *and grey* 190 K*. The parameters used were as described in Section 3.8, the device parameters for the simulation was* $L = 150$*. It should be noted these parameters does not take Ir(ppy)$_2$acac into account.*

In Figure 4.9 the measurements show the same agreement with the simulation as in Figure 4.7, however this is less clear for the measurements at a temperature of 250 K and 230 K. This might be due to the hysteresis effect of forward and backward scans solely under positive bias.

4.4 Carrier density

In Figure 4.10, the effect of higher current densities on the polaron (carrier) density at $T = 300$ across the active layer is shown. Comparison of the curves in Figure 4.10, in the order of increasing J, shows that the point of minimal carrier density moves away from the middle of the active layer [11]. This effect is as a result of higher electric fields at higher current densities. A explanation could be: a higher electric field, increases the drift contribution in Equation

(2.7), it pushes the charge carriers, in case for holes, from anode to cathode. Hence, shifting the minimum to the right.

The position of the minimum polaron density shows where possibly the point of minimal TPQ could be. Since TPQ is linear with the polaron density as well as the triplet density, optical simulations were ran in order to determine the triplet density profile at t = 0 in the active layer. Furthermore, to determine the photoluminescence efficiency, not only the TPQ needs to be determined, but the outcoupling as well.

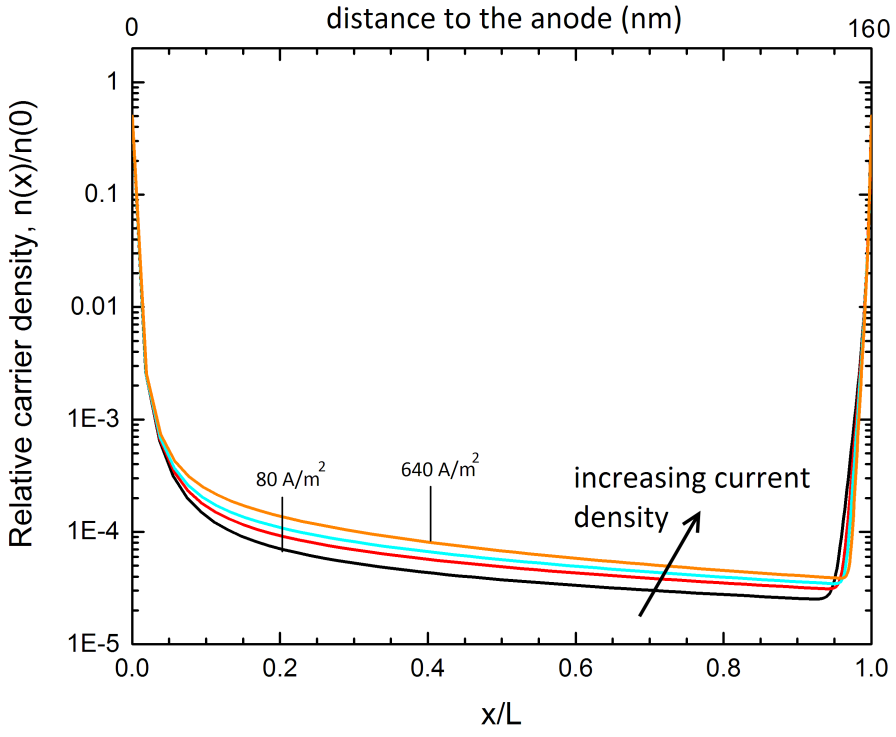

Figure 4.10: The polaron density in TCTA at various current densities, for L = 160. The device which contains TCTA is symmetric. In black the polaron density at 80 A/m^2, red at 160 A/m^2, turquoise at 300 A/m^2 and orange at 640 A/m^2.

4.5 Optical simulation

Firstly the results of the optical outcoupling of the matrix stack is given and discussed. Next the incoupling of the matrix stack is used to calculate the triplet density profile at $t = 0$.

Outcoupling

In order to simulate the outcoupling of light out of the active layer Setfos was configured as explained in Section 4.5. The software was then used to determine the radiance as function of the measurement angle and emitter location, for a given emitter spectrum shown in Appendix C. This can also be done as a post-processing step, by selecting a white emitter spectra in Setfos and taking the convolution of the Setfos spectrum and emitter spectrum. The resulting spectrally integrated Figure is shown in Figure 4.11, in this Figure the emitter location with high radiance slightly moves to the left with increasing angle. This can be due to a longer optical path length inside the media at increasing angles, as well as consequence of refraction between layers.

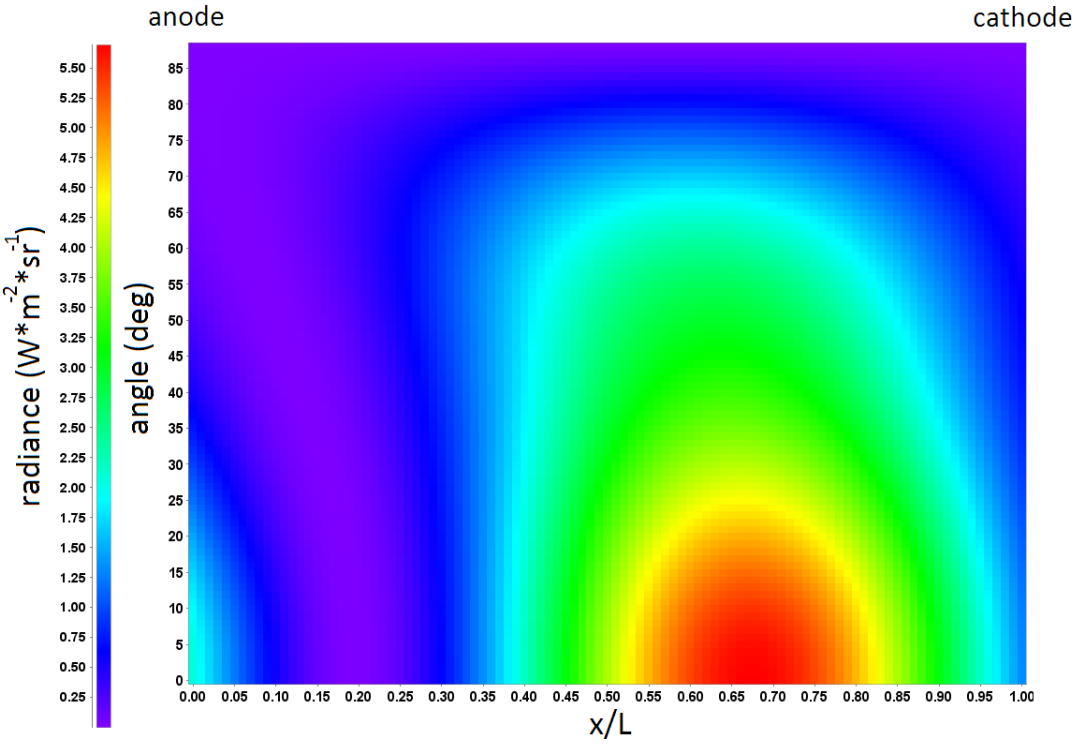

Figure 4.11: Heat map of radiance as function of normalized dipole position and angle w.r.t. normal of substrate. Colour of the heat map changes gradually from purple to red, with purple indicating no radiance and red indicating maximal radiance. Data was retrieved from Setfos, with the settings of Setfos as described in Section 3.9 and an active layer thickness of 160 nm.

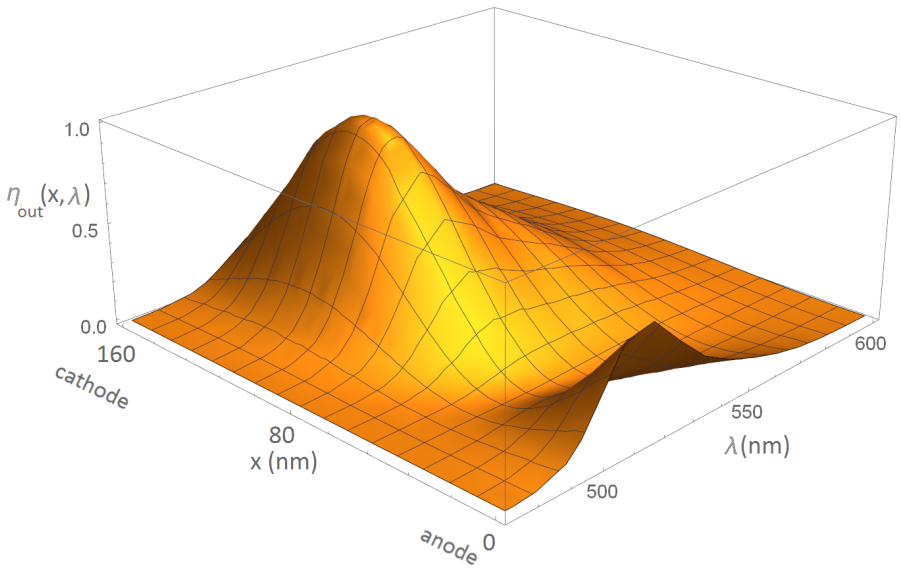

Figure 4.12: The outcoupling normalized at the maximum as function of the wavelength and normalized position (x/L), with $L = 160\,\text{nm}$. Data was retrieved from Setfos, with the settings of Setfos as described in Section 3.9 and an active layer thickness of 160 nm.

Next, the angle is fixed at 0 degrees analogous to the experimental setup of a typical PL measurement setup. At an angle of 0 degrees the radiance can then be simulated as function of the wavelength and position, yielding Figure 4.12. It can be seen that the position where maximal outcoupling occurs moves as function of the wavelength, this is due to the wavelength dependent attenuation of the materials in the stack.

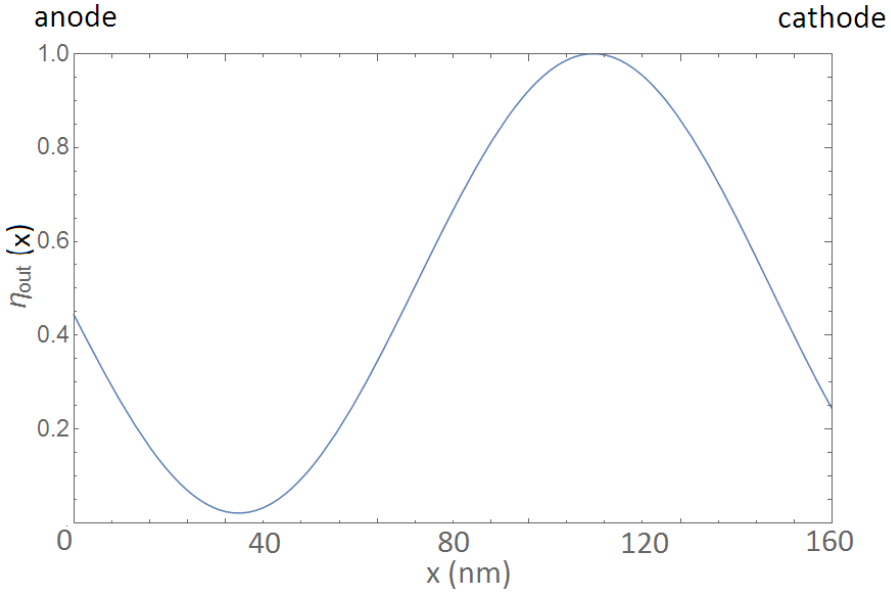

Figure 4.13: The outcoupling normalized at the maximum as function of the normalized position (x/L). Data was retrieved from Setfos, with the settings of Setfos as described in Section 3.9 for devices with 160 nm *active layer. The data was then integrated over the wavelength.*

The outcoupling efficiency for an ideal detector, can be found by spectrally integrating Figure 4.12, resulting Figure 4.13. However, if the used detector isn't equally sensitive for all wavelengths, the outcoupling can be defined as,

$$\eta_{out}(x) = \int_0^\infty S(\lambda) \cdot \eta_{out}(x, \lambda)\, \mathrm{d}\lambda, \tag{4.1}$$

with $S(\lambda)$ the sensitivity of the detector and $\eta_{out}(x, \lambda)$ the outcoupling factor as function of λ and x.

The first anti node is expected to be a quarter of the internal emission wavelength (75 nm).[30] However, the aluminium cathode does not act a perfect electric conductor and light or electromagnetic waves will penetrate this material. This results in the first antinode to be placed a bit closer to the aluminum cathode, less than 75 nm. Indeed Figure 4.13 shows that the maximal outcoupling is less than 75 nm away from the cathode. It is determined from Figure 4.13 that the first antinode is 57 nm away from the aluminium cathode.

Incoupling

With the same settings as described in Section 4.5, Setfos was configured and used to determine the position where most of the absorption occurs inside the active layer. Furthermore, Setfos was configured for a laser, with a laser wavelength of 337 nm. This laser is set to hit the sample 45 degrees w.r.t. the normal of the sample, so the angle is fixed at 45 degrees. The resulting incoupling profile can be found in Figure 4.14, there it is shown that the incoupling has a high triplet density near the interface anode-active layer. While the polaron density is highest a bit away from the electrode-active layer interface, this leads to a lot of quenching at the anode-active layer interface according to Equation (2.5). There is a global maximum at x =

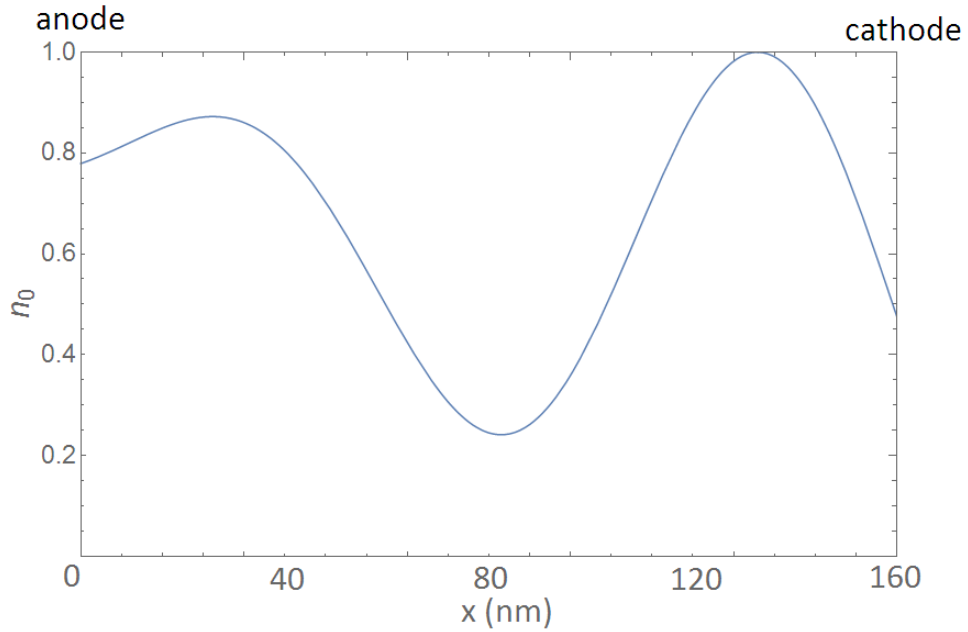

Figure 4.14: The incoupling or triplet density profile at t=0 as function of the normalized position (x/L), calculated for devices with active layer of 160 nm. The settings used were as described in Section 4.5

133 nm. Whereas the carrier density at x = 133 nm at all J's in Figure 4.10 are low, these two effects combined leads, according to Equation (2.5), to a relatively low quenching at the point of maximal incoupling. The point of maximal incoupling is also the point where the triplet density is the highest, this could lead to a high TPQ, however due to the low polaron density it is relatively low. The high carrier density found near the anode-active layer interface shows up to few orders of magnitude higher TPQ. It is then expected that most of the quenching x/L $<$ 0.5, however the outcoupling is low for emitters positioned at x/L $<$ 0.5. Thus, the PL efficiency is decreased very little even though a lot of quenching occurs at x/L $<$ 0.5.

4.6 Triplet-polaron quenching rate

It was aimed to combine the calculation model with the optical model, with this combined model real world measurements can be translated into a TPQ rate coefficient using the steps described in Section 2.7. The resulting TPQ rate coefficient at various current densities can be found in Figure 4.15, the PL measurement data was retrieved from Ref.[24]. It should be noted that the devices used did not have PEDOT:PSS and it was shown in this work that devices without PEDOT:PSS have bad agreement with the simulation at the voltages used in that PL experiment. Furthermore, the calculated polaron density profile does not take trap sites into account. This means that the calculation method needs to be adjusted, allowing the presence of trap sites to be considered. This absence of trap sites in the calculation method will result in an overestimation of amount of charge carriers. To recapitulate, the devices without PEDOT:PSS showed a higher current density at all voltages and the polaron density profile overestimates the amount of charge carriers.

Nevertheless, the polaron density is assumed to be correct in order to complete a first analysis of the unique approach used in this work. The final results of this unique approach is given in Figure 4.15 and shows that the TPQ rate coefficient is not constant. This observation is in contrast to what generally is believed.[14;31;32;33] While, the Purcell effect is not included in the analysis, which could possibly increase the TPQ rate coefficient, by lowering the radiative life time of a triplet state. There is no reason for this effect to be a decreasing function of the

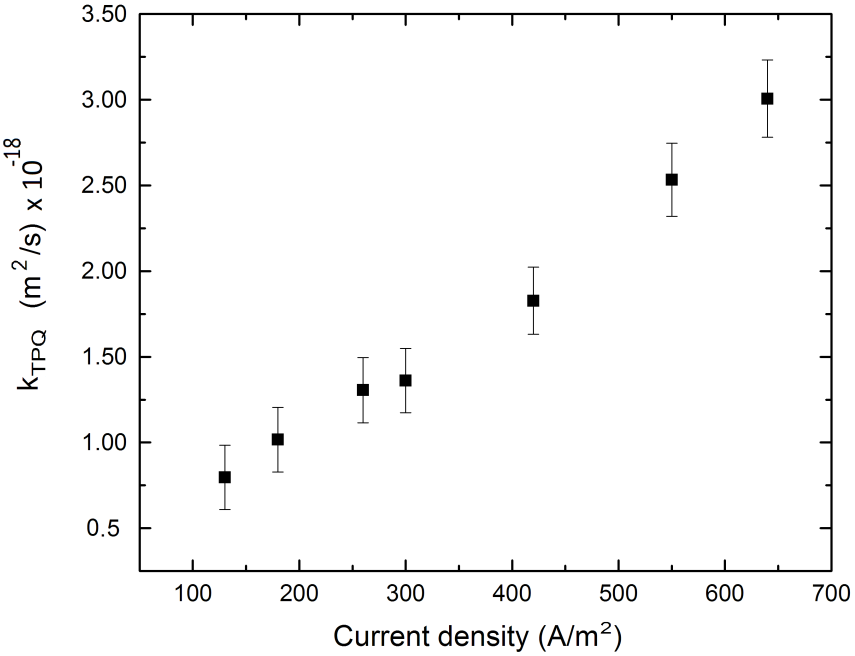

Figure 4.15: The triplet-polaron quenching rate coefficient as function of the current density. PL measurement was done on devices with an active layer of 160 nm TCTA and 4 wt. % $Ir(ppy)_2acac$, with the setup described in Section 2.7.

current density, negating the seemingly linear increase in the rate coefficient as function of the current density as shown in Figure 4.15. This linear increase in the TPQ rate coefficient might indicate that more physical processes are playing a role and the simple rate equation given in Equation (2.5) describes exciton physics inadequately.

5 Conclusion

In this study it was key to combine multiple approaches for a complete triplet-polaron quenching model. This study has used the calculation model of Van Mensfoort and Coehoorn [11] and an optical simulation model. To start off, the device yield has increased with the use of PEDOT:PSS. This implies that the interface between ITO and MoOx had defects which would show as bad device yield or as inconsistent devices. The thicknesses of the devices without and with dye molecules were determined to be (134 ± 1) nm and (150 ± 1) nm, respectively. These thicknesses are in accordance what was expected from the deposition settings of these devices. Furthermore from current density-voltage measurements under ambient conditions good agreement with the calculational model has been found for voltages over 5 V. The degree of trapping has been found the be a factor 2-3. This is due to the matching of the highest occupied molecular orbitals of the semiconductor and dye molecule (dopant), both are 5.6 eV. From the temperature dependent measurements from 190 K up to 270 K similar agreement has been found as in the case of ambient temperature (300 K) measurement. There was noticeable presence of hysteresis in the studied devices.

Next, is the optical simulations. In this approach the amount of light that is absorbed and escaped is simulated with Setfos. It was found for horizontal dipole moment orientation that the outcoupling is maximal at a position of of 110 nm, for an active layer of 160 nm. Indeed, as expected this is about a quarter internal emission wavelength from the cathode. Furthermore, most of the light escapes at normalized position (x/L) > 0.5, while most of the light is absorbed at a position of 133 nm. Thus, the highest triplet density at t = 0 is found at a position of 133 nm. This coincides with the region where most light escapes and also the region where the carrier density is minimal, which increases from the middle to the cathode with increasing bias voltage. In total this leads to a low TPQ in the region with high optical outcoupling.

It would be interesting to vary the active layer thicknesses such that the point of maximal triplet density overlaps with minimal carrier density, it is also interesting to mismatch these two points. The insight needed for this practice can be achieved with help of Setfos simulations of the incoupling and outcoupling profiles. The results will verify the calculation model, if indeed by matching and mismatching, a higher and lower PL efficiency is found respectively, then the simulated polaron density should be comparable to the polaron density found in real devices. Also, the calculation method can be improved. Currently it does not take trap sites into account. Hence, a disagreement between the measurement and calculation results was found. From the improved calculation method, a lower current density is expected at voltages over 5 V compared with the used calculation method in this work.

Lastly, the combined model has successfully been used to yield results for 160 nm devices with 4 wt. % $Ir(ppy)_2acac$ and no PEDOT:PSS. It was shown that that the k_{TPQ} was not constant. This result shows either that an erroneous polaron density was calculated or that TPQ is not described adequately through a rate coefficient as argued at the beginning of this work. A successful analysis using a unique approach for studying triplet-polaron quenching in organic phosphorescent devices was achieved.

References

[1] P. W. Wiessner, Proceedings of the National Academy of Sciences **111**, 14027 (2014).

[2] A. J. Heeger, Current Applied Physics **1**, 247 (2001).

[3] H. Shirakawa, Reviews of Modern Physics **73**, 713 (2001).

[4] H. v. Eersel, *Device physics of organic light-emitting diodes : interplay between charges and excitons* (Technische Universiteit Eindhoven, Eindhoven, 2015).

[5] M. Mazur, D. Kaczmarek, J. Domaradzki, D. Wojcieszak, S. Song, and F. Placido, Conference Proceedings - The 8th International Conference on Advanced Semiconductor Devices and Microsystems, ASDAM 2010 , 65 (2010).

[6] R. Coehoorn, L. Zhang, P. A. Bobbert, and H. Van Eersel, Physical Review B **95**, 1 (2017).

[7] H. Van Eersel, P. A. Bobbert, R. A. J. Janssen, and R. Coehoorn, Applied Physics Letters **105** (2014), 10.1063/1.4897534.

[8] A. Köhler and H. Bässler, Electronic Processes in Organic Semiconductors , 1 (2015).

[9] A. Köhler and H. Bässler, Materials Science and Engineering R: Reports **66**, 71 (2009).

[10] H. Bassler, "Charge Transport in Disordered Organic Photoconductors a Monte Carlo Simulation Study," (1993).

[11] S. L. M. Van Mensfoort and R. Coehoorn, Physical Review B - Condensed Matter and Materials Physics **78** (2008), 10.1103/PhysRevB.78.085207.

[12] N. Tessler, Y. Preezant, N. Rappaport, and Y. Roichman, "Charge transport in disordered organic materials and its relevance to thin-film devices: A tutorial review," (2009).

[13] Y. Kawamura, K. Goushi, J. Brooks, J. J. Brown, H. Sasabe, and C. Adachi, Applied Physics Letters **86**, 1 (2005).

[14] M. A. Baldo, C. Adachi, and S. R. Forrest, Physical Review B - Condensed Matter and Materials Physics **62**, 10967 (2000).

[15] T. Forster, Die Naturwissenschaften **33**, 166 (1946).

[16] M. Furno, R. Meerheim, S. Hofmann, B. Lüssem, and K. Leo, Physical Review B - Condensed Matter and Materials Physics **85**, 1 (2012).

[17] M. A. Baldo, R. J. Holmes, and S. R. Forrest, Physical Review B - Condensed Matter and Materials Physics **66**, 353211 (2002).

[18] W. F. Pasveer, J. Cottaar, C. Tanase, R. Coehoorn, P. A. Bobbert, P. W. Blom, M. De Leeuw, and M. A. Michels, Physical Review Letters **94**, 206601 (2005).

[19] A. Massé, P. Friederich, F. Symalla, F. Liu, V. Meded, R. Coehoorn, W. Wenzel, and P. A. Bobbert, Physical Review B **95**, 115204 (2017).

[20] H. Van Eersel, P. A. Bobbert, R. A. J. Janssen, and R. Coehoorn, Journal of Applied Physics **119**, 1 (2016).

[21] K. A. Neyts, Journal of the Optical Society of America A **15**, 962 (1998).

[22] C. Adachi, M. A. Baldo, M. E. Thompson, and S. R. Forrest, Journal of Applied Physics **90**, 5048 (2001).

[23] A. Perumal, H. Faber, N. Yaacobi-Gross, P. Pattanasattayavong, C. Burgess, S. Jha, M. A. McLachlan, P. N. Stavrinou, T. D. Anthopoulos, and D. D. C. Bradley, Advanced Materials **27**, 93 (2015).

[24] P. Castenetto, *Experimental study of exciton-polaron quenching processes in phosphorescent organic host-guest materials used in OLEDs*, Tech. Rep. (Universite de namur, 2017).

[25] K. Marinus, *Comparison between experimental and simulated hole transport in organic material TCTA Bachelor final project*, Tech. Rep. (Technische Universiteit Eindhoven, 2016).

[26] F. McCrackin, E. Passaglia, R. Stromberg, and H. Steinberg, Journal of Research of the National Institute of Standards and Technology **67A**, 363 (1963).

[27] L. Hanssen, Applied optics **40**, 3196 (2001).

[28] K. H. Kim, C. K. Moon, J. H. Lee, S. Y. Kim, and J. J. Kim, Advanced Materials **26**, 3844 (2014).

[29] S. L. M. van Mensfoort, M. Carvelli, M. Megens, D. Wehenkel, M. Bartyzel, H. Greiner, R. a. J. Janssen, and R. Coehoorn, Nature Photonics **4**, 329 (2010).

[30] G. Björk, S. MacHida, Y. Yamamoto, and K. Igeta, Physical Review A **44**, 669 (1991).

[31] T. Serevičius, R. Komskis, P. Adomènas, O. Adomènienè, G. Kreiza, V. Jankauskas, K. Kazlauskas, A. Miasojedovas, V. Jankus, A. Monkman, and S. Juršènas, Journal of Physical Chemistry C **121**, 8515 (2017).

[32] Q. Wang, I. W. H. Oswald, M. R. Perez, H. Jia, B. E. Gnade, and M. A. Omary, Advanced Functional Materials **23**, 5420 (2013).

[33] D. Hertel and K. Meerholz, Journal of Physical Chemistry B **111**, 12075 (2007).

[34] P. Mutsaers, *Experimentele fysica 1 lecture notes*, Tech. Rep. (Technische Universiteit Eindhoven, Eindhoven, 2016).

Appendices

A Cleaning procedures

A.1 Cleaning blank glass samples

In order to clean glass samples the samples were soaked in different solvents. The cleaning was accelerated using a sonic bath, the order of solvents can be found in Table 2. Afterwards the samples were dried with pressurized nitrogen, received 15 minutes ultraviolet-ozone (UV-ozone) treatment and the last 2 minutes were dedicated to flushing the machine with ambient air.

Table 2: Cleaning procedure for glass samples, with time of the sonic bath in minutes. In order of ascending steps and repeated for every sample.

Step	Solvent	Time
1	Soap	10
2	Demineralised water	5
3	Acetone	10
4	Isopropanol	10

A.2 Cleaning ITO glass samples

The cleaning of ITO glass samples was done in a different way than blank glass samples described in A.1. The ITO samples were treated with the techniques described in Table 3. Afterwards the samples were dried with pressurized nitrogen, received 30 minute UV-ozone treatment and the last 2 minutes were dedicated to flushing the machine with ambient air.

Table 3: Cleaning procedure for ITO samples, with method the equipment used and time in minutes. In order of ascending steps and repeated for every sample.

Step	Method	Action or Solvent	Time
1	Sonic bath	Soap	10
2	Gloves	Scrubbing	1
3	Sonic bath	Soap	15
4	Flushing	Deminaralised water	30
5	Sonic bath	Acetone	30

B Error analysis

The average of a set of data ($\bar{x}$) of N entries is given by,

$$\bar{x} = \frac{\sum_i^N x^{[i]}}{N} \tag{App.1}$$

100% error interval

Error analysis in the 100% reliabilty domain is found by Equation (App.2), taken from [34]. This is used for all error calculations except when differently noted.

$$\Delta x = \sum_i \left| \frac{\partial f}{\partial x^{[i]}} \right| \Delta x^{[i]} \tag{App.2}$$

This means for a small discrete data set x of $N < 10$ entries, the error of the average is given by,

$$\Delta\bar{x} = \frac{R}{2\sqrt{N}}. \tag{App.3}$$

With R the range, given as,

$$R = max\{x\} - min\{x\} \tag{App.4}$$

68% error interval

Error analysis in the 68% reliabilty domain is found by Equation (App.5), taken from [34].

$$S_x = \sqrt{\sum_i \left(\frac{\partial f}{\partial x^{[i]}} S_{x^{[i]}} \right)^2} \tag{App.5}$$

For a big data set x of $N > 10$ entries, the data can be considered normally distributed, thus the error of the average is given by,

$$\Delta\bar{x} = \frac{\sigma}{\sqrt{N}}. \tag{App.6}$$

With σ the standard deviation, given as,

$$\sigma = \sqrt{\frac{\sum_i \left(x^{[i]} - \bar{x}\right)^2}{N}} \tag{App.7}$$

C Emission spectrum of $Ir(ppy)_2acac$

The emission spectrum used in Setfos is given in Figure I.

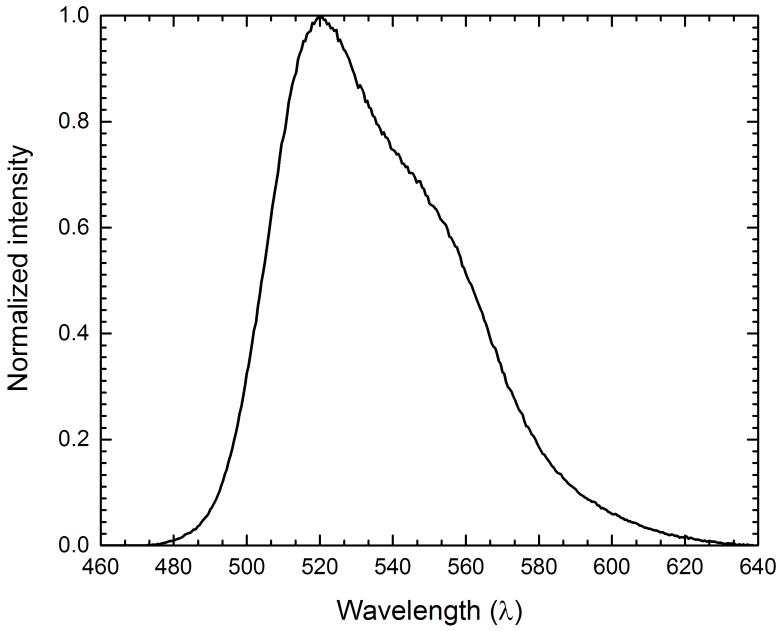

Figure I: The emission spectrum of $Ir(ppy)_2acac$ on a quartz substrate, normalized such that the maximum is unity.

D Mathematica script

1D drift-diffusion simulation of the current density in single-layer single-carrier sandwich-type devices

Bonham-Jarvis method. Type-I systems. Random Gaussian DOS.

I. Parameter initialization and pre-processing

```
(* Calculation of the current-voltage curves for a single-
 carrier device with drift and diffusion, *)
(* for a single layer with a GAUSSIAN density of
 states. Extension of the method given in ref. 1 *)
(* Calculation for a situation in which there is a minimum in the carrier density *)
(* in each of the layers in the device. *)
(* Version of the program with the enhancement
 of the diffusion coefficient according to the *)
(* generalized Einstein equation, and with the field dependence of the mobility. *)
(* The method is explained in ref. 5. Please refer to that
 paper when publishing results obtained using this notebook. *)
(* [1]. J.S. Bonham and D.H. Jarvis, Austr. J. Chem. 30, 1977, 705-720 *)
(* [2]. R. Coehoorn et al., Phys. Ref B 72, 155206, (2005). *)
(* [3]. F. Pasveer et al., Phys. Rev. Lett. 94, 206601 (2005). *)
(* [4]. Y. Roichman and N. Tessler, Appl. Phys. Lett. 80, 1948 (2002). *)
(* [5]. S.L.M. van Mensfoort and R. Coehoorn, Phys. Rev. B 78, 085207 (2008). *)

SetDirectory["C:\\Users\\Ryuuta\\Documents\\Tu EHV\\OLED\\Simulations"]
tstart = TimeUsed[];
(* Parameters defining the numerecial precision *)
ioprec = 80;
wp = 30;
ag = 25;
pg = 22;

(* Physical constants *)
e = SetPrecision[1.6021766 * 10^-19, ioprec]; (* electron charge, in C *)
kb = SetPrecision[1.3806485 * 10^-23, ioprec]; (* Boltzmann constant, in J/K *)
eps0 = SetPrecision[8.85419 * 10^-12, ioprec];
(* vacuum dielectric permittivity, in S.I. units *)

(*constants from paper for mobility enhancement*)

(*Nothing*)(*
B=SetPrecision[1.9,ioprec]; (*constant B*)
A=SetPrecision[0.57/B,ioprec]; (* constant A*)
Cconst=SetPrecision[0.41,ioprec]; (*constant C*)
mu0star=SetPrecision[6.1*10^-6,ioprec];
(* Mobility in limit of zero field, zero carrier density and  no disorder*)
*)
(*SX^CORR*)
```

```
B = SetPrecision[2.7, ioprec]; (*constant B*)
A = SetPrecision[0.81 / B, ioprec]; (* constant A*)
Cconst = SetPrecision[0.40, ioprec]; (*constant C*)
mu0star = SetPrecision[7.6 * 10^-6, ioprec];
(* Mobility in limit of zero field, zero carrier density and  no disorder*)

(*Custom*)
sigmainev = 0.136;
punten = 51; (*Amount of simulation points for J-V curve*)
lremoveFaster[lst_List] := Replace[lst, {l_List} :> l, {0, Infinity}];
(*Choose your current range in log*)
machtmin = -2;
machtmax = 4 - machtmin;

(* Experimental conditions *)
T = SetPrecision[300, ioprec]; (* absolute temperature, in K *)

(* Material and device parameters *)
L = SetPrecision[135 * 10^-9, ioprec]; (* layer thickness, in m *)
Nt = SetPrecision[0.87 * 10^27, ioprec]; (* volume density of molecules, in m^-3 *)
sigma = SetPrecision[sigmainev * e, ioprec]; (* width of the Gaussian DOS, in J *)
sbykt = SetPrecision[sigma / (kb * T), ioprec]; (* disorder parameter, dimensionless *)
mu0t = SetPrecision[mu0star * Exp[-Cconst * sbykt^2], ioprec];
mu0 = SetPrecision[mu0t, ioprec]; (* mobility in the limit of zero ca
 rrier density and field *)
epsr = SetPrecision[3.0, ioprec]; (* relative dielectric constant *)
eps = SetPrecision[eps0 * epsr, ioprec]; (* dielectric permittivity *)
Print["Disorder parameter sbykt = ", N[sbykt, 7]];
Print["μ_0= ", NumberForm[mu0, 5] , " mobility in the limit of zero ca
    rrier density and fields"];

(* Calculation of the Fermi energy as a function of the carrier concentration  *)
ClearAll[ef, nbynt];
mmax = 1000;
nbyntmin = SetPrecision[10^-15, ioprec];
nbyntmax = SetPrecision[0.5, ioprec];
lognbyntmin = SetPrecision[Log[10, nbyntmin], ioprec];
lognbyntmax = SetPrecision[Log[10, nbyntmax], ioprec];
efmin = SetPrecision[(Log[nbyntmin] - sbykt^2 / 2) / sbykt, ioprec];
(* This guarantees that the concentration range includes c = nbyntmin *)
efmax = SetPrecision[0, ioprec];
Do[{
        ef[m] = SetPrecision[efmin + (efmax - efmin) * m / mmax, ioprec];
        nbynt[m] = SetPrecision[0, ioprec] ;
        nbynt[m] = NIntegrate[1 / Sqrt[2 Pi] *
      Exp[-eee^2 / 2] / (1 + Exp[(eee - ef[m]) * sbykt]), {eee, -Infinity, Infinity}] ;
    },
         {m, 0, mmax}];
tabnef = Table[{nbynt[m], ef[m]}, {m, 0, mmax}];
funcef = Interpolation[tabnef];
```

```
tabefn = Table[{ef[m], nbynt[m]}, {m, 0, mmax}];
funcn = Interpolation[tabefn];

(* Calculation of the mobility enhancement
 as a function of the carrier concentration (EGDM) *)
Do[{
    lognbynt = SetPrecision[lognbyntmin + (lognbyntmax - lognbyntmin) * m / mmax, ioprec];
    nbynt[m] = SetPrecision[10.0^lognbynt, ioprec] ;
        delta = SetPrecision[2/sbykt^2 (Log[sbykt^2 - sbykt] - Log[Log[4]]), ioprec];
    (* see eq. 3(c) in ref. 2 *)
  mubymu0[m] = SetPrecision[Exp[1/2 * (sbykt^2 - sbykt) * (2 * nbynt[m])^delta], ioprec];
    (* eqs 31 and D4 in ref. 2 *)
    },
        {m, 0, mmax}];

(* Calculation of the diffusion constant enhancement
 (a) as a function of the carrier concentration  *)
Do[{
    lognbynt = SetPrecision[lognbyntmin + (lognbyntmax - lognbyntmin) * m / mmax, ioprec];
    nbynt[m] = SetPrecision[10.0^lognbynt, ioprec] ;
        ClearAll[ee];
  a[m] =
    SetPrecision[nbynt[m] * Sqrt[2 * Pi] /
        NIntegrate[Exp[-ee^2 / 2] *
          Exp[(ee - funcef[nbynt[m]]) * sbykt] / (1 + Exp[(ee - funcef[nbynt[m]]) * sbykt])^2,
         {ee, -Infinity, +Infinity}], ioprec],
    },
        {m, 0, mmax}];

(* Plot enhancement functions *)
tab1 = Table[{nbynt[m], a[m] * mubymu0[m]}, {m, 0, mmax}];
tab2 = Table[{nbynt[m], mubymu0[m]}, {m, 0, mmax}];
tab3 = Table[{nbynt[m], a[m]}, {m, 0, mmax}];
(* func1 is the diffusion constant enhancement,
as a function of nbynt, with respect to D = (kb*T/e)*mu0. *)
(* func2 is the mobility enhancement as a function of nbynt; not used in program *)
(* func3 is the diffusion constant enhancement,
as a function of nbynt, with respect to D = (kb*T/e)*mu. *)
func10 = Interpolation[tab1];
func20 = Interpolation[tab2];
func30 = Interpolation[tab3];
nbyntstar = SetPrecision[0.1, ioprec];

ClearAll[func1, func2, func3];
func1[x_] := 1 /; (x < nbyntmin);
func1[x_] := func10[x] /; (nbyntmin ≤ x ≤ nbyntstar);
```

```
func1[x_] := func10[nbyntstar] /; (x > nbyntstar);
func2[x_] := 1 /; (x < nbyntmin);
func2[x_] := func20[x] /; (nbyntmin <= x ≤ nbyntstar);
func2[x_] := func20[nbyntstar] /; (x > nbyntstar);
nbyntstara = SetPrecision[1 / 2, ioprec];
func3[x_] := 1 /; (x ≤ nbyntmin);
func3[x_] := func30[x] /; (nbyntmin < x ≤ nbyntstara);
func3[x_] := func30[nbyntstara] /; (x > nbyntstara);

Print["Diffusion constant and mobility
    enhancement as a function of nbynt, on a double-log scale."];
Print["Full: diffusion constant enhancement (a*mubymu0),
    with respect to D = (kb*T/e)*mu0. "];
Print["Dashed: mobility enhancement (mubymu0), obtained using the compact model. "];
ClearAll[x];
Print[Plot[{Log[10, func1[10^x]], Log[10, func2[10^x]]},
   {x, -10, 10}, PlotRange -> {{-10, 10}, {0, 6}}, Frame -> True,
   PlotStyle -> {Dashing[{1, 0}], Dashing[{0.02, 0.02}]}]];

Print["Diffusion coefficient enhancement function
    (a[nbynt]), with respect to D = (kb*T/e)*mu, lin-log scale."];
Print[Plot[func3[10^x], {x, -10, +10}, PlotRange -> {{-10, 10}, {0, 10}},
   Frame -> True, PlotStyle -> {Dashing[{1, 0}]}]];

(* Field dependence of the mobility, as given by eq. (3) in ref. 3 (EGDM). *)
(* For large fields,
the enhancement function is taken equal to the value at a reduced field of 2, *)
(* in order to more optimally describe the numerical data in ref. (3). *)
(* Note that the carrier concentration dependence of this function *)
(* (see the inset in fig. 3 of ref. 3) is neglected. *)
Fieldboundary = SetPrecision[2.0 * (sigma / e) * Nt^(1/3), ioprec];
mufieldlow[Field_] :=
  SetPrecision[Exp[A * (sbykt^(3/2) - 2.2) * (Sqrt[1 + B * (Field * e * Nt^(-1/3) / sigma)^2] - 1)], ioprec];
mufieldhigh[Field_] := SetPrecision[Exp[A * (sbykt^(3/2) - 2.2) * (Sqrt[1 + B * (2)^2] - 1)], ioprec];
mufield[Field_] := mufieldlow[Field] /; (Abs[Field] <= Fieldboundary);
mufield[Field_] := mufieldhigh[Field] /; (Abs[Field] > Fieldboundary);

(* Settings for the case of a constant mobility *)
(*
ClearAll[mufield,mufieldprime,funcn];
mufield[Field_]:=1 ;
mufieldprime[Field_]:=0;
ClearAll[func1,func2,func3];
func1[x_]:=1 ; func2[x_]:=1; func3[x_]:=1; funcn[x_]:=Exp[x*e/(kb*T)];
*)

Print["tused = ", TimeUsed[] - tstart, " CPU seconds"];
```

```
(*Define the file names for next section*)
jvout = StringJoin["sxcorrjv", TextString[Round[machtmin * 10]], "tot",
    TextString[Round[(machtmax + machtmin) * 10]], "dikte=", TextString[Round[L * 10^9]],
    "nm", "punten=", TextString[Round[punten]], "T=", TextString[Round[T]], ".xls"];
fjout = StringJoin["sxcorrfj", TextString[Round[machtmin * 10]], "tot",
    TextString[Round[(machtmax + machtmin) * 10]], "dikte=", TextString[Round[L * 10^9]],
    "nm", "punten=", TextString[Round[punten]], "T=", TextString[Round[T]], ".xls"];
```

II. The actual simulation, for a chosen set of current density values.

```
(* Start calculation of J(V) curve *)
(* Only solutions for which f[y] has a minimum
 within the layer are considered (type-I cases). *)
(* Extension 0 refers to the minimum in the y[f] curve. *)
(* The search starts by performing calculations
 for the interval boundaries f0min and f0max. *)
(* Subsequently, a next trial value of f0 is selected by
 linear interpolation of Log[10,J] versus f0, *)
(* using the last and one-but last results. *)
(* Each next calculation (for a larger current density)
 is started with selfconsistent value of f0 from the *)
(* calculation for the previous current density as the value f0min. *)
(* The example given below corresponds to the device studied in fig. 6(b) of ref. 5 *)

tstart = TimeUsed[];

(* The boundary conditions can be entered by specifying an injection barrier Delta, *)
(* and then calculating the carrier concentrations
 nbynt0 and nbyntL at the anode and cathode, respectively, *)
(* or by directly entering these carrier concentrations. Here,
the latter option is used. *)
nbynt0 = SetPrecision[0.5, ioprec]; (* carrier concentration at the anode,
0.5 si égalité entre les deux car symmétrique *)
nbyntL = SetPrecision[0.5, ioprec]; (* carrier concentration at the cathode *)
Delta0 = SetPrecision[funcef[nbynt0] * sigma / e, ioprec];
(* injection barrier at the anode interface *)
DeltaL = SetPrecision[funcef[nbyntL] * sigma / e, ioprec];
(* injection barrier at the cathode interface *)
Vbi = SetPrecision[(funcef[nbynt0] - funcef[nbyntL]) * sigma / e, ioprec];
(* built-in voltage *)
Print["The carrier concentration at the anode, neglecting the image charge effect, is ",
  N[nbynt0, 5], " ."];
Print["The carrier concentration at the cathode, neglecting
    the image charge effect, is ", N[nbyntL, 5], " ."];
Print["The injection barrier at the anode and cathode interfaces is  ",
  N[Delta0, 5], " eV and ", N[DeltaL, 5], " eV, respectively"];
Print["V_bi = ", N[Vbi, 5], " (V)."];
```

```
Print[];
Print[];

(* Chose the boundary values of f such that the
 values of f at the anode and cathode fall certainly *)
(* within the interval [fboundmin;fboundmax] *)
fboundmin = SetPrecision[-10^9, ioprec];
fboundplus = SetPrecision[10^9, ioprec];

(* Iterative calculation of (J,V) points *)
ClearAll[J, Vec, Ves];
imax = punten; (* number of J(V) points *)
kmax = 51; (* maximum number of iterations per J(V) point *)
(* Definition of the first two trial values of fb, for i = 1 and k = 1,2 *)
(*fbtrial[1,1]=SetPrecision[1.73,ioprec];
fbtrial[1,2]=SetPrecision[1.75,ioprec];*)
fbtrial[1, 1] = SetPrecision[0.01, ioprec];
fbtrial[1, 2] = SetPrecision[0.05, ioprec];



Do[{
   If[imax > 1, Jfixed[i] = SetPrecision[3 * 10^(machtmin+machtmax*(i-1)/(imax-1)), ioprec]];
   (* Changing bounds current density,
   amount of simulation points need to be changed accordingly. *)
   If[imax == 1, Jfixed[i] = SetPrecision[1.7 * 10^0.0, ioprec]];
   Print["******* Jfixed = ", N[Jfixed[i], 5], " (A/m^2) *******"];
   const1 = SetPrecision[((eps * e/(kb*T))^(1/3) (Jfixed[i]/mu0)^(2/3))/(e * Nt), ioprec];
   (* ratio between nbynt and y *)
   const2 = SetPrecision[((kb * T)/e Jfixed[i]/(eps * mu0))^(1/3), ioprec];
   (* ratio between the field F and f *)
   (* ymax= SetPrecision[nbynt0/const1,ioprec]; *)
   ymax = SetPrecision[0.5/const1, ioprec]; (* changed 30-1-2008 *)
   If[i == 2, fbtrial[i, 1] =
     fbtrial[i - 1, kfinal] + 0.9 * (Log[10, Jfixed[i]] - Log[10, Jfixed[i - 1]])/slope];
   If[i == 2, fbtrial[i, 2] = fbtrial[i - 1, kfinal] +
     1.1 * (Log[10, Jfixed[i]] - Log[10, Jfixed[i - 1]])/slope];
   If[i > 2, fbtrial[i, 1] = fbfinal[i - 1] + 0.9 * (fbfinal[i - 1] - fbfinal[i - 2])];
   If[i > 2, fbtrial[i, 2] = fbfinal[i - 1] + 1.1 * (fbfinal[i - 1] - fbfinal[i - 2])];

   Do[{
     fb = SetPrecision[fbtrial[i, k], ioprec];
     fbfinal[i] = SetPrecision[fb, ioprec];
     Print["fb = ", fb];
     ClearAll[y0, y, f, yrule];
     yzerorule =
```

```
FindRoot[fb/func3[const1 * y0] == 1/(func1[const1 * y0] * mufield[const2 * fb] * y0,
  {y0, 10^-9, ymax}, WorkingPrecision → 80, AccuracyGoal → 30, MaxIterations → 1000];
yzero = y0 /. yzerorule;
Print["yzero = ", yzero];
yrule = NDSolve[
  {y'[f] == f/func3[const1 * y[f]] - 1/(func1[const1 * y[f]] * mufield[const2 * f] * y[f],
   y[fb] == yzero}, y, {f, fboundmin, fb},
  WorkingPrecision → 80, AccuracyGoal → 12, MaxSteps -> 200000];
solutionmin = y /. First[yrule];
   ClearAll[y, f, yrule];
   yrule = NDSolve[
  {y'[f] == f/func3[const1 * y[f]] - 1/(func1[const1 * y[f]] * mufield[const2 * f] * y[f],
   y[fb] == yzero}, y, {f, fb, fboundplus},
  WorkingPrecision → 80, AccuracyGoal → 9, MaxSteps -> 200000];
solutionplus = y /. First[yrule];
   Print[Jfixed[i], "   ", yzero, "  ", const1 * yzero, "  ", const2 * fb];
   If[yzero < 0, {Print["Break, because yzero < 0"], Break[]}];

(* Determination of the values of
 f that correspond to the boundary conditions n0 and nL *)
 ClearAll[f, fanoderule];
 fanoderule = FindRoot[const1 * solutionmin[f] == nbynt0, {f, fboundmin, fb},
  WorkingPrecision → 41, AccuracyGoal → 9, MaxIterations → 300];
 fanode = f /. fanoderule;
 ClearAll[f, fcathoderule];
 fcathoderule = FindRoot[const1 * solutionplus[f] == nbyntL, {f, fb, fboundplus},
  WorkingPrecision → 42, AccuracyGoal → 9, MaxIterations → 300];
 fcathode = f /. fcathoderule;
Print["fanode = ", N[fanode, 5],
 "       fcathode = ", N[fcathode, 5]];
 If[fanode < 0.8 * fboundmin, {Print["fanode < fboundmin", fanode],
  fboundmin = 3/2 * fboundmin}];
 If[fcathode > 0.8 * fboundplus, {Print["fcathode> fboundplus", fcathode],
  fboundplus = 3/2 * fboundplus}];

ymin = SetPrecision[solutionmin[fanode], ioprec];
yplus = SetPrecision[solutionplus[fcathode], ioprec];
(* below: check whether the boundaries are
  situated at points of high density, close or just above nbyntstar *)

term1 = SetPrecision[NIntegrate[1/solutionmin[f], {f, fanode, fb},
   WorkingPrecision → 40, AccuracyGoal → 9, MaxRecursion -> 40], ioprec];
term2 = SetPrecision[NIntegrate[1/solutionplus[f], {f, fb, fcathode},
   WorkingPrecision → 40, AccuracyGoal → 9, MaxRecursion -> 10], ioprec];
curr = SetPrecision[(term1 + term2)^3, ioprec];
volt =
```

```
      SetPrecision[NIntegrate[f / solutionmin[f] , {f, fanode, fb}, MaxRecursion -> 10] +
        NIntegrate[f / solutionplus[f] , {f, fb, fcathode}], ioprec];

    J[i] = SetPrecision[mu0 * eps * (kb * T)^2 / (e^2 L^3) * curr, ioprec];

    (*Explicit expression for carrier density
      temp=SetPrecision[eps*kb*T/(e^2*L^2)*curr^(2/3)*y/Nt/.First[yrule],ioprec];
    n[i]=temp/.
      Print["carrier density = ",N[n[i],5]];

    Finding the position *)
    spos = SetPrecision[NIntegrate[1 / (curr^(1/3) solutionmin[f]), {f, fanode, fb},
       WorkingPrecision → 40, AccuracyGoal → 9, MaxRecursion -> 40], ioprec];
    xpos[i] = SetPrecision[(*L**)spos, ioprec];
    Print["relative x position in device = ", N[xpos[i], 5]];

    Ves[i] = kb * T / e * volt; (* electrostatic potential difference *)
    Vec[i] = Ves[i] + Vbi; (* electrochemical potential difference *)
    If[k == k,
     Print["V_el.chem. = ",     N[Vec[i], 5],      " (V)      V_el.stat. = ",
      N[Ves[i], 5],              " (V)      J = ",
      N[J[i], 5] ,     " (A/m^2)    J/J_fixed = ", N[J[i] / Jfixed[i], 5]]];
    If[Abs[J[i] / Jfixed[i] - 1.0] < 0.005, Print["nbynt_minimum = ", N[yzero * const1, 5],
      "  nbynt_anode = ", N[ymin * const1, 5], "  nbynt_cathode = ", N[yplus * const1, 5]]];
    If[Abs[J[i] / Jfixed[i] - 1.0] < 0.005, Print[""]];
    If[Abs[J[i] / Jfixed[i] - 1.0] < 0.005, Print[""]];
    If[Abs[J[i] / Jfixed[i] - 1.0] < 0.005,
     {fbj[i] = {J[i], fb}, listfj = Array[fbj, imax]}];
    If[Abs[J[i] / Jfixed[i] - 1.0] < 0.005, Break[]];

    LJout[i, k] = SetPrecision[Log[10, J[i]], ioprec];

  If[k ≥ 2,
      {slope = SetPrecision[
         (LJout[i, k] - LJout[i, k - 1]) / (fbtrial[i, k] - fbtrial[i, k - 1]), ioprec];
       fbtrial[i, k + 1] = SetPrecision[(Log[10, Jfixed[i]] - LJout[i, k - 1]) / slope +
          fbtrial[i, k - 1], ioprec];
       kfinal = k + 1}];

    Print["End of loop: k = ", k, "     fbtrial = ", N[fbtrial[i, k], 5]];
    Print[" "];
   }, {k, 1, kmax}],
 }, {i, 1, imax}];
jvll = Table[{Log[10, Vec[i]], Log[10, J[i]]}, {i, 1, imax}];

Print[
  "Print and plot of the current density as a function of the voltage (double-10-log)"];

SetDirectory["C:\\Users\\Ryuuta\\Documents\\Tu EHV\\OLED\\Simulations\\jv"]
```

```
(*J-v save map*)
jv = Table[{Vec[i], J[i]}, {i, 1, imax}];
Export[jvout, jv, "XLS"]

SetDirectory["C:\\Users\\Ryuuta\\Documents\\Tu EHV\\OLED\\Simulations\\fj"]
(*field over j save map*)

Export[fjout, listfj, "XLS"]

plotjv =
  Print[ListPlot[jvll, PlotRange → {{-2, 1.3}, {0, 7}}, Frame → True, Joined → True]];

Print["tused = ", TimeUsed[] - tstart, " CPU seconds"];
```

III. Setting up field over current density

```
(* Plot of the carrier density across
  the device for the (J,V) point obtained for k = kmax *)
(* FINAL and OPTIMAL result. No warnings,
no oscillations in the carrier concentration. *)
(* Result obtained in conjunction with the use of WorkingPrecision→50,
AccuracyGoal→30 in NDSolve in the main program*)
tstart = TimeUsed[];
ClearAll[ff, solution, xbyLmin];

importnamefj =
  StringJoin["C:\\Users\\Ryuuta\\Documents\\Tu EHV\\OLED\\Simulations\\fj\\", fjout];
listfj = Import[importnamefj, "Data"];
listfj = lremoveFaster[listfj];

(* interpolation and visual check*)
fmin = SetPrecision[Interpolation[listfj, InterpolationOrder → 1], ioprec];

(*
ListPlot[listfj]
 Plot[fmin[x],{x,30,800}]
*)

Jfix = SetPrecision[260, ioprec];
(* Choose for which current density the carrier density needs to be found *)
fb = SetPrecision[fmin[Jfix], ioprec];
Print["dimensionless field at minimum carrier density is ", N[fb]]
(* define solutions *)
ClearAll[y0, y, f, yrule];
```

```
(*pre work for carrier density *)

const1 = SetPrecision[ (eps * e/(kb*T))^(1/3) (Jfix / mu0)^(2/3) / (e * Nt), ioprec];
(* ratio between nbynt and y *)
const2 = SetPrecision[ (kb * T / e  Jfix / (eps * mu0))^(1/3), ioprec];
(* ratio between the field F and f *)

yzerorule = FindRoot[ fb / func3[const1 * y0] == 1 / (func1[const1 * y0] * mufield[const2 * fb] * y0),
  {y0, 10^-9, ymax}, WorkingPrecision → 80, AccuracyGoal → 30, MaxIterations → 1000];
yzero = y0 /. yzerorule;
Print["yzero = ", yzero];
yrule =
  NDSolve[{y'[f] == f / func3[const1 * y[f]] - 1 / (func1[const1 * y[f]] * mufield[const2 * f] * y[f]),
    y[fmin[Jfix]] == yzero}, y, {f, fboundmin, fmin[Jfix]},
   WorkingPrecision → 80, AccuracyGoal → 12, MaxSteps -> 20000];
solutionmin = y /. First[yrule];
ClearAll[y, f, yrule];
yrule =
  NDSolve[{y'[f] == f / func3[const1 * y[f]] - 1 / (func1[const1 * y[f]] * mufield[const2 * f] * y[f]),
    y[fmin[Jfix]] == yzero}, y, {f, fmin[Jfix], fboundplus},
   WorkingPrecision → 80, AccuracyGoal → 9, MaxSteps -> 20000];
solutionplus = y /. First[yrule];

ClearAll[f, fanoderule];
fanoderule = FindRoot[const1 * solutionmin[f] == nbynt0, {f, fboundmin, fb},
   WorkingPrecision → 41, AccuracyGoal → 9, MaxIterations → 300];
fanode = f /. fanoderule;
ClearAll[f, fcathoderule];
fcathoderule = FindRoot[const1 * solutionplus[f] == nbyntL,
   {f, fb, fboundplus}, WorkingPrecision → 42,
   AccuracyGoal → 9, MaxIterations → 300];
fcathode = f /. fcathoderule;

ymin = SetPrecision[solutionmin[fanode], ioprec];
yplus = SetPrecision[solutionplus[fcathode], ioprec];

term1 = SetPrecision[NIntegrate[1 / solutionmin[f], {f, fanode, fb},
    WorkingPrecision → 40, AccuracyGoal → 9, MaxRecursion -> 40], ioprec];
term2 = SetPrecision[NIntegrate[1 / solutionplus[f], {f, fb, fcathode},
    WorkingPrecision → 40, AccuracyGoal → 9, MaxRecursion -> 10], ioprec];
curr = SetPrecision[(term1 + term2)^3, ioprec];
```

Carrier density

```
(* Calculate carrier density as func of x *)

ClearAll[ff, solution, ffieldxbyL];

solution[ff_, J_] := solutionmin[ff] /; (fanode ≤ ff < fmin[J]) ;
solution[ff_, J_] := solutionplus[ff] /; (fmin[J] ≤ ff ≤ fcathode) ;
xbyLmin =
  SetPrecision[NIntegrate[1 / (curr^(1 / 3) solutionmin[ff]), {ff, fanode, fmin[Jfix]},
    WorkingPrecision → wp, AccuracyGoal → 30, MaxRecursion -> 40], ioprec];

ClearAll[ff, ffield];

(* concatinating functions induces integration error,
seperating functions prevents this *)

int1[ffieldxbyL_?NumericQ] :=
  int1[ffieldxbyL] = NIntegrate[1 / solutionmin[ff], {ff, fanode, ffieldxbyL},
    WorkingPrecision → 80 , AccuracyGoal → 30, MaxRecursion → 20];
int2[J_?NumericQ] := int2[J] = NIntegrate[1 / solutionmin[ff], {ff, fanode, fmin[J]},
    WorkingPrecision → 80, AccuracyGoal → 30, MaxRecursion → 20];
int3[ffieldxbyL_?NumericQ, J_] := int3[ffieldxbyL, J] =
   NIntegrate[1 / solutionplus[ff], {ff, fmin[J], ffieldxbyL},
    WorkingPrecision → 80, AccuracyGoal → 30, MaxRecursion → 20];

(* Solving for the field *)

ffield[xbyL_, J_] :=
  SetPrecision[(ffieldxbyL /. FindRoot[ int1[ffieldxbyL] == xbyL * curr^(1/3), {ffieldxbyL,
        fanode, fmin[J]}, MaxIterations → 1000]) , ioprec] /; (xbyL < xbyLmin);
ffield[xbyL_, J_] := SetPrecision[(ffieldxbyL /. FindRoot[




Print[""];
Print["The carrier concentration across the device for the (J,V)
    point obtained for k = kmax. Minimum at x/L = ", N[xbyLmin, 8]];

imax = 50; (*amount of points, very important fotr accuracy*)
nbynty = SetPrecision[ ((eps * e/(kb*T))^(1/3) (Jfix / mu0)^(2/3)) / (e * Nt), ioprec];

tabmin = Quiet[Parallelize[Table[{xbyLmin * i / imax,
      nbynty * solution[ffield[xbyLmin * i / imax, Jfix], Jfix]}, {i, 1, imax - 1}]]];
tabmax = Quiet[Parallelize[Table[{xbyLmin + (1 - xbyLmin) * (i / imax), nbynty * solution[
        ffield[xbyLmin + (1 - xbyLmin) * (i / imax), Jfix], Jfix]}, {i, 0, imax - 1}]]];


Print["tused = ", TimeUsed[] - tstart, " CPU seconds"];
```

Outcoupling model

```
(* Calculate carrier density as func of x *)

ClearAll[ff, solution, ffieldxbyL];

solution[ff_, J_] := solutionmin[ff] /; (fanode ≤ ff < fmin[J]) ;
solution[ff_, J_] := solutionplus[ff] /; (fmin[J] ≤ ff ≤ fcathode) ;
xbyLmin =
  SetPrecision[NIntegrate[1 / (curr^(1 / 3) solutionmin[ff]), {ff, fanode, fmin[Jfix]},
    WorkingPrecision → wp, AccuracyGoal → 30, MaxRecursion -> 40], ioprec];

ClearAll[ff, ffield];

(* concatinating functions induces integration error,
seperating functions prevents this *)

int1[ffieldxbyL_?NumericQ] :=
  int1[ffieldxbyL] = NIntegrate[1 / solutionmin[ff], {ff, fanode, ffieldxbyL},
    WorkingPrecision → 80 , AccuracyGoal → 30, MaxRecursion → 20];
int2[J_?NumericQ] := int2[J] = NIntegrate[1 / solutionmin[ff], {ff, fanode, fmin[J]},
    WorkingPrecision → 80, AccuracyGoal → 30, MaxRecursion → 20];
int3[ffieldxbyL_?NumericQ, J_] := int3[ffieldxbyL, J] =
   NIntegrate[1 / solutionplus[ff], {ff, fmin[J], ffieldxbyL},
    WorkingPrecision → 80, AccuracyGoal → 30, MaxRecursion → 20];

(* Solving for the field *)

ffield[xbyL_, J_] :=
  SetPrecision[(ffieldxbyL /. FindRoot[int1[ffieldxbyL] == xbyL * curr^(1/3), {ffieldxbyL,
        fanode, fmin[J]}, MaxIterations → 1000]) , ioprec] /; (xbyL < xbyLmin);
ffield[xbyL_, J_] := SetPrecision[(ffieldxbyL /. FindRoot[
        int2[J] + int3[ffieldxbyL, J] == xbyL * curr^(1/3), {ffieldxbyL, fmin[J], fcathode},
        MaxIterations → 1000] ), ioprec]; /; (xbyL >= xbyLmin);

Print[""];
Print["The carrier concentration across the device for the (J,V)
    point obtained for k = kmax. Minimum at x/L = ", N[xbyLmin, 8]];

imax = 50; (*amount of points, very important fotr accuracy*)
nbynty = SetPrecision[ (eps * e/(kb*T))^(1/3) (Jfix / mu0)^(2/3) / (e * Nt), ioprec];

tabmin = Quiet[Parallelize[Table[{xbyLmin * i / imax,
      nbynty * solution[ffield[xbyLmin * i / imax, Jfix], Jfix]}, {i, 1, imax - 1}]]];
tabmax = Quiet[Parallelize[Table[{xbyLmin + (1 - xbyLmin) * (i / imax), nbynty * solution[
        ffield[xbyLmin + (1 - xbyLmin) * (i / imax), Jfix], Jfix]}, {i, 0, imax - 1}]]];


Print["tused = ", TimeUsed[] - tstart, " CPU seconds"];
```

Outcoupling model

```
(*Does not need to be rerun*)
ClearAll[tempimport, x, λ, test, inter, uitmatrix, uitinter, uitnorm, uitint, maxval]
λbegin = 473; (*Begin of wavelength list*)
λend = 650; (*End of wavelength list*)

tempimport = Import["C:\\Users\\Ryuuta\\Documents\\Tu
      EHV\\OLED\\Simulations\\setfos\\emissionparallel.xlsx", "XLSX"];
(*folder with setfos outcoupling matrix, in excel sheet*)
uitkoppelingimport = lremoveFaster[tempimport];
uitnietnorm[λ_, x_] :=
  uitkoppelingimport[[(λ - λbegin + x) * 100 + 1]][[3]] /; (λbegin ≤ λ ≤ λend);

maxval[λ_] := Max[Table[uitnietnorm[λ, 0.01 * i], {i, 0, 100}]]
maxvalue = Max[Table[uitnietnorm[j, 0.01 * i], {i, 0, 100}, {j, λbegin, λend, 1}]];
uitdisc[λ_, x_] := If[maxval[λ] > 0,
  uitkoppelingimport[[(λ - λbegin + x) * 100 + (λ - λbegin + 1)]][[4]] / maxvalue, 0]

test = Table[{i, uitdisc[518, i]}, {i, 0, 1, 0.01}];
inter = Interpolation[test, InterpolationOrder → 1];

uitmatrix =
  Flatten[Table[{{λ, x}, uitdisc[λ, x]}, {λ, λbegin, λend, 1}, {x, 0, 1, 0.01}], 1];
(*Re-code this step for higher efficiency, by better element verwijzing*)
uitinter = Interpolation[uitmatrix, InterpolationOrder → 1];
(*Wavelength only defined for 473-638, while position from 0-1*)
(*Optional, visual check*)
Plot[inter[x], {x, 0, 1}]
Plot3D[uitinter[x, y], {x, 473, 600}, {y, 0, 1},
 AxesLabel → {Style["λ(nm)", Black, FontSize → 40], Style[x, Black, FontSize → 40],
   Style[η, Black, FontSize → 40]}, TicksStyle → FontSize → 30]
```

Integration over all wavelengths outcoupling and incoupling

```
(*Does not need to be rerun*)
uitintnotnormed[x_] := Integrate[uitinter[λ, x], {λ, 473, 638}];
uitnorm = NMaximize[{uitintnotnormed[x], 0.1 < x < 0.9}, {x}];
ηout[x_] := uitintnotnormed[x] / uitnorm[[1]];
(*Incoupling interpolation*)
ClearAll[n0]
beginin = 234;
endin = 392;
deltain = endin - beginin;
tempimportin = Import[
    "C:\\Users\\Ryuuta\\Documents\\Tu EHV\\OLED\\Simulations\\setfos\\160nm\\Absorption
      profile 160 nm.txt", "Data"]; (*Incoupling from setfos*)
maxvalin = Max[tempimportin[[beginin ;; endin, 2]]];
inmatrix =
  Table[{i / (deltain), tempimportin[[beginin + i, 2]] / maxvalin}, {i, 0, deltain}];
n0 = Interpolation[inmatrix, InterpolationOrder → 1];

(*Plot of outcoupling and then incoupling*)
Plot[ηout[x], {x, 0, 1}, PlotRange → {{0, 1}, {0, 1}}, Frame → True,
 LabelStyle → {FontSize → 30}, FrameLabel → {x, ηout}, FrameTicksStyle → 24]
Plot[n0[x], {x, 0, 1}, PlotRange → {{0, 1}, {0, 1}}, Frame → True,
 LabelStyle → {FontSize → 30}, FrameLabel → {x, n0}, FrameTicksStyle → 24]
```

TPQ model

```
(*preamble*)
ClearAll[x, t, J, nt, np, τ, sol, solnorm, i, imax]
τ = SetPrecision[1.37 * 10^-6, ioprec];
imax = 3;
ηstart = 0.885;

(*interpolation of data *)
nptable = Join[{{0, nbynt0}}, tabmin, tabmax, {{1, nbyntL}}];
outpol = StringJoin["poldenscorrsx", TextString[Round[Jfix]], ".xls"];
np = SetPrecision[Interpolation[nptable, InterpolationOrder → 1], ioprec];

(* visualize and check validity of interpolation *)
ListPlot[nptable]
```

```
LogPlot[np[x], {x, 0, 1}]
```

```
nt[x_, t_, J_] := If[J == 0, n0[x] * Exp[-t / τ], n0[x] * Exp[-t / τ - ktpq * np[x, J] * t]] ;

IPL[t_, J_] :=
  NIntegrate[ηout[x] * nt[x, t, J], {x, 0, L}, WorkingPrecision → 30, AccuracyGoal → 10];

ηpl[J_] := NIntegrate[IPL[t, J] / IPL[t, 0], {t, 0, ∞}];
(*
(* simple case, for n0 and nout not a func of x and given J *)
simplesol= NIntegrate[ (τ^-1) (1/τ+ktpq*np[x]*Nt)^-1,
  {x,0,1} ,WorkingPrecision→42,AccuracyGoal→10];
(*
ClearAll[ktpq]
  solnorm = FindRoot[simplesol==0.9, {ktpq,0},
  WorkingPrecision→42,AccuracyGoal→9,MaxIterations→300];
sol= ktpq/.solnorm
*)

 Do[{ClearAll[ktpq],
   simpleroot = FindRoot[simplesol==ηstart+0.01(i-2),
     {ktpq,0},WorkingPrecision→50,AccuracyGoal→10,MaxIterations→300];
   solsimple[i]= SetPrecision[ktpq/.simpleroot ,ioprec]},
  {i,1,imax}]

 koutsimple=Table[{ηstart+0.01(i-2),N[solsimple[i],6]},{i,1,imax}];
outsimple=StringJoin["solSimplektpqcorrsx",TextString[Round[Jfix]],".xls"];

(*In case that incoupling is not a function of the position. A solution then is:*)
asol= NIntegrate[ηout[x]*(τ^-1)*(1/τ+ktpq*np[x]*Nt)^-1, {x,0,1} ,
   WorkingPrecision→42,AccuracyGoal→10]/NIntegrate[ηout[x],{x,0,1}];

 Do[{ClearAll[ktpq],
   aroot=FindRoot[asol==ηstart+0.01(i-2),{ktpq,0}];
   sola[i]= SetPrecision[ktpq/.aroot ,ioprec]},
  {i,1,imax}]

 kouta=Table[{ηstart+0.01(i-2),N[sola[i],6]},{i,1,imax}];
outa=StringJoin["solAktpqcorrsx",TextString[Round[Jfix]],".xls"];
*)
(*Complete equation*)
bsol = NIntegrate[ηout[x] * n0[x] * (τ^-1) * (1 / τ + ktpq * np[x] * Nt)^-1, {x, 0, 1} ,
    WorkingPrecision → 42, AccuracyGoal → 10] / NIntegrate[ηout[x] * n0[x], {x, 0, 1}];

Do[{ClearAll[ktpq],
  broot = FindRoot[bsol == ηstart + 0.01 (i - 2), {ktpq, 0}];
  sola[i] = SetPrecision[ktpq /. broot , ioprec]},
```

```
 {i, 1, imax}]

koutb = Table[{ηstart + 0.01 (i - 2), N[sola[i], 6]}, {i, 1, imax}];
outb = StringJoin["solBktpqcorrsx", TextString[Round[Jfix]], ".xls"];
(*
SetDirectory["C:\\Users\\Ryuuta\\Documents\\Tu EHV\\OLED\\Simulations\\ktpq\\Simple"];
Export[outsimple,koutsimple,"XLS"];

SetDirectory["C:\\Users\\Ryuuta\\Documents\\Tu EHV\\OLED\\Simulations\\ktpq\\A"];
Export[outa,kouta,"XLS"];
*)

SetDirectory["C:\\Users\\Ryuuta\\Documents\\Tu EHV\\OLED\\Simulations\\ktpq\\B"];
(*Save map for KTPQ*)
Export[outb, koutb, "XLS"];

SetDirectory["C:\\Users\\Ryuuta\\Documents\\Tu EHV\\OLED\\Simulations\\ktpq\\polaron"];
(*Save map for polaron density as function of position*)
Export[outpol, nptable, "XLS"];
```